Geophysical Journal International Advance Access published September 8, 2016

Efficiency of perfectly matched layers for seismic wave modeling in second-order viscoelastic equations

by

Ping Ping[1,2,7], Yu Zhang[3,4,5], Yixian Xu[6,7] and Risheng Chu[1,2]

[1]State Key Laboratory of Geodesy and Earth's Dynamics
Wuhan, 430077, China

[2]Institute of Geodesy and Geophysics
Chinese Academy of Sciences
Wuhan, 430077, China

[3]School of Geodesy and Geomatics
Wuhan University
Wuhan, 430079, China

[4]Key Laboratory of Geospace Environment and Geodesy
Ministry of Education
Wuhan, 430079, China

[5]Collaborative Innovation Center for Geospatial Technology
Wuhan University
Wuhan 430079, China

[6]School of Earth Sciences, Zhejiang University,
Hangzhou, 310027, China

[7]Hubei Subsurface Multi–scale Imaging Key Laboratory (SMIL), Institute of Geophysics and Geomatics
China University of Geosciences
Wuhan, 430074, China

∗Corresponding Author:
Ping Ping (ppingapple@gmail.com or pingping@whigg.ac.cn)
Yu Zhang (yuz124@gmail.com)
Yixian Xu (xyxian65@aliyun.com)
Risheng Chu (chur@asch.whigg.ac.cn)

Submitted for consideration of publication in
Geophysical Journal International
March 31, 2016
Revised and resubmitted for consideration of publication in
Geophysical Journal International
August 10, 2016

Summary

In order to improve the perfectly matched layer (PML) efficiency in viscoelastic media, we firstly propose a split multi-axial PML (M-PML) and an unsplit convolutional PML (C-PML) in the second-order viscoelastic wave equations with the displacement as the only unknown. The advantage of these formulations is that it is easy and efficient to revise the existing codes of the second-order spectral element method (SEM) or finite element method (FEM) with absorbing boundaries in a uniform equation, as well as more economical than the auxiliary differential equations PML (ADEPML). Three models which are easily suffered from late time instabilities are considered to validate our approaches. Through comparison the M-PML with C-PML efficiency of absorption and stability for long time simulation, it can be concluded that: 1) For an isotropic viscoelastic medium with high Poisson's ratio, the C-PML will be a sufficient choice for long time simulation because of its weak reflections and superior stability; 2) Unlike the M-PML with high-order damping profile, the M-PML with 2nd-order damping profile loses its stability in long time simulation for an isotropic viscoelastic medium; 3) In an anisotropic viscoelastic medium, the C-PML suffers from instabilities, while the M-PML with 2nd-order damping profile can be a better choice for its superior stability and more acceptable weak reflections than the M-PML with high-order damping profile. The comparative analysis of the developed methods offers meaningful significance for long time seismic wave modeling in second-order viscoelastic wave equations.

Key words: Elasticity and anelasticity; Instability analysis; Numerical modeling; Wave propagation; Computational seismology.

1. INTRODUCTION

In the context of numerical modeling of seismic wave propagation in unbounded media, as in the case of simulations performed at the local, regional, or continental scale, wave energy needs to be absorbed at the artificial boundaries of the computation region and therefore nonreflecting conditions must be defined at these boundaries to mimic an unbounded medium. The perfectly matched layer (PML) introduced by Bérenger (1994) has been theoretically confirmed to possess excellent absorption performance for a wave with arbitrary incidence angle. The field variables of the PML are split into nonphysical components, which make it possible to incorporate mathematical formulations for desired absorption. Because of the advantages of PML, it was rapidly reformulated in different wave propagation modeling problems and adapted to acoustic (e.g., Hu, 1996; Hesthaven, 1998; Nataf, 2006), elastic (e.g., Chew & Liu, 1996; Hastings et al., 1996; Collino & Tsogka, 2001; Festa & Nielsen, 2003; Basu & Chopra, 2004), poroelastic (Zeng et al. 2001; Martin et al. 2008), and viscoelastic media (Bécache et al., 2004; Martin & Komatitsch, 2009). Some researchers also engaged into anisotropic effects on PMLs (e.g., Bécache et al., 2001; Martin et al., 2009; Meza-Fajardo & Papageogiou, 2008; Kreiss & Duru, 2013; Ping et al., 2014a).

A recurring problem in the context of the use of a discrete PML is that the reflection coefficient is not zero after discretization, but more importantly, it becomes very large at grazing incidence (Collino & Monk, 1998; Winton & Rappaport, 2000) and unstable for long time simulations (Festa et al., 2005). These problems have been intensively investigated in recent years (Halpern et al., 2011). For example, it was initially regarded as the constitutive parameters unsatisfying causality making dynamical instability of the classical PML

(Kuzuoglu & Mittra, 1996), due to the divergence of the PML solution under small perturbations (Abarbanel & Gottlieb, 1998). Kuzuoglu and Mittra (1996) proposed the complex frequency-shifted PML (CFS-PML) using a frequency dependent stretching function. The CFS-PML was first implemented in a split-field formulation (Gedney, 1996). Then, several PMLs were proposed for an unsplit-field by using different implementation of the CFS-PML, e.g., the matched Z-transform CFS-PML (MZT CFS-PML) (Shi et al., 2012), the ADE CFS-PML using auxiliary differential equations (Wang & Liang, 2006; Kristek et al., 2009; Qin et al., 2009; Gedney & Zhao, 2010; Martin et al., 2010; Zhang & Shen, 2010; Duru & Kreiss, 2012; Feng & Li, 2013; Duru, 2014; Xie et al., 2014), and the C-PML using convolution terms (Gedney, 1996; Zhao & Cangellaris, 1996; Ziolkowski, 1997; Abarbanel & Gottlieb, 1998; Basu & Chopra, 2004; Appelö & Kreiss,2005; Komatitsch & Martin, 2007; Li & Matar, 2010; Matzen, 2011), which were all found to be efficient in absorbing evanescent waves and near-grazing incident waves. Besides, Fathi et al. (2015) developed a hybrid treatment which coupled an unsplit-field PML, but in displacement-stress formulations, to a standard displacement-only formulation in the regular region.

Komatitsch and Martin (2007) introduced a simple unsplit version of such a convolutional PML (C-PML) for the elastic case. Martin et al. (2008) extended it to the poroelastic case and the viscoelastic case (Martin & Komatitsch, 2009). This C-PML technique has also been extended to heterogeneous anisotropic models in the presence of curved interfaces and a free surface using a high-order finite-element method (Martin et al., 2009). It improves the absorption of reflected waves at grazing incidences (Roden & Gedney, 2000; Bérenger, 2002; Festa et al., 2005; Komatitsch & Martin, 2007; Martin & Komatitsch, 2009). However, for

elastic or viscoelastic media, these C-PMLs mentioned above are based upon the first-order mixed displacement/velocity–stress wave equations. Matzen (2011) developed a C-PML for the second-order elastic wave equations without auxiliary memory variables. Xie et al. (2014) provided a new treatment to remove singular parameters in the auxiliary differential equations of PML (ADEPML), which can be applied to high-order SEM but with more storage consumption than Matzen's (2011). Gao et al. (2015) also proposed an unsplit CFS-PML using auxiliary differential equations just for second-order elastic wave equations. However, the high order methods abovementioned are all based upon the elastic wave equations, which cannot straightforwardly applied in viscoelastic media. The C-PML in the second-order viscoelastic wave equations with displacements as the only unknown still needs to be reconstructed.

The multi-axial PML (M-PML) method was also developed to tackle the late time instability of PML, which is efficient and stable without dependence on frequencies and directions of wave propagation (Meza-Fajardo & Papageorgiou, 2008, 2010, 2012; Ping et al., 2014a, 2014b). The M-PML may be not perfectly matched, but it is applied to anisotropic elastic media with good performance (Dmitriev & Lisitsa, 2011, 2012) and keeps superior stability in late time simulation. The M-PML method has also been verified more stable and efficient than classical PML and C-PML in long time simulation for wave propagation in isotropic and anisotropic elastic media with the first-order equations (Meza-Fajardo & Papageorgiou, 2008). Zhang et al. (2014) combined the CFS-PML and the M-PML to derive an ADE CFS-MPML to avoid the PML amplification in anisotropic elastic media for the first-order wave equations. We extended the M-PML adapted in first-order wave equations to

second-order elastic wave equations (Ping et al., 2014a). It improves the instabilities in long time simulation for isotropic with high Poisson's ratio and anisotropic elastic media. The extension of this approach in second-order viscoelastic wave equation will be firstly further introduced and investigated in this research.

Therefore, all of the PMLs used in the context of the viscoelastic wave equations are in the spatial first-order systems with displacement-stress or velocity-stress formulations (Bécache et al., 2004; Martin & Komatitsch, 2009). The PML formulations for the first-order scheme cannot be applied directly to the second-order system. Meanwhile, the PMLs for second-order wave equations are all for elastic media and are inappropriate to viscoelastic wave equations. It appears that the PML formulations in second-order wave equations in viscoelastic media have still to be suggested. In this paper, we develop the C-PML used in the second-order viscoelastic wave equations with economical computational consumption, for its exclusion of auxiliary memory variables and easily using the second-order SEM and FEM without entire reconstruction of the existed codes. We also further rewrite and introduce M-PML formulations in second-order wave equations in viscoelastic media, which has been mentioned but not been discussed in details (Ping et al., 2014b). Meanwhile, the convolution approach used in this paper is more accurate than that in our previous research (Ping et al., 2014b). In general, we present the M-PML and C-PML formulations for FEM and SEM simulations based upon the second-order viscoelastic seismic wave equations with displacements as the only unknown that have never been discussed before. Furthermore, through the comparison between two specific improved PMLs, we try to favor an optimal PML choice in second-order viscoelastic wave equations in such the isotropic media with

high Poisson's ratio and anisotropic media, with regard to the efficiency of absorption and stability for a long time simulation.

2. FORMULATION OF PMLS IN VISCOELASTIC MEDIA

2.1 Wave equations in viscoelastic media

The constitutive relation for a linear viscoelastic medium can be expressed as (Carcione, 2015)

$$\begin{aligned} T_I &= [A_{IJ} + A_{IJ}^{(v)}\chi_v(0)]\varepsilon_J(t) + A_{IJ}^{(v)}\sum_{l=1}^{Lv}\varphi_{vl}(t) * \varepsilon_J \\ &= H_{IJ}\varepsilon_J(t) + A_{IJ}^{(v)}\sum_{l=1}^{Lv}\varphi_{vl}(t) * \varepsilon_J, \end{aligned} \tag{1}$$

where A_{IJ} and $A_{IJ}^{(v)}$ depend on unrelaxed stiffnesses c_{IJ} ($I, J = 1 \sim 6$), T_I and ε_J represent stress and strain tensors, Lv represents the number of Zener viscoelastic elements, and

$$\chi_v(t) = Lv\left(\sum_{l=1}^{Lv}\frac{\tau_{\varepsilon l}^{(v)}}{\tau_{\sigma l}^{(v)}}\right)^{-1}\left[1 - \frac{1}{Lv}\sum_{l=1}^{Lv}\left(1 - \frac{\tau_{\varepsilon l}^{(v)}}{\tau_{\sigma l}^{(v)}}\right)\exp(-t/\sigma_{\sigma l}^{(v)})\right], v = 1, 2, \tag{2a}$$

$$\varphi_{vl}(t) = \left(\tau_{\sigma l}^{(v)}\sum_{l=1}^{Lv}\frac{\tau_{\varepsilon l}^{(v)}}{\tau_{\sigma l}^{(v)}}\right)^{-1}\left[1 - \frac{\tau_{\varepsilon l}^{(v)}}{\tau_{\sigma l}^{(v)}}\right]\exp(-t/\sigma_{\sigma l}^{(v)}), \tag{2b}$$

The qualities $\chi_v(v = 1, 2)$ are dimensionless relaxation functions for quasi-dilatational and quasi-shear modes, respectively. $\tau_{\varepsilon l}^{(v)}$ and $\tau_{\sigma l}^{(v)}$ ($l = 1 \sim Lv$) are material relaxation time parameters, and $\tau_{\varepsilon l}^{(v)} \geq \tau_{\sigma l}^{(v)}$.

Eq. (1) also can be rewritten in form of matrix by the geometry relations $\boldsymbol{\varepsilon} = \frac{1}{2}\left(\nabla \mathbf{s} + \nabla^T \mathbf{s}\right)$ as

$$\mathbf{T} = \mathbf{H} : \frac{1}{2}\left(\nabla \mathbf{s} + (\nabla \mathbf{s})^T\right) + \mathbf{A}^v : \left[\sum_{l=1}^{Lv}\varphi_{vl} * \frac{1}{2}\left(\nabla \mathbf{s} + (\nabla \mathbf{s})^T\right)\right], \tag{3}$$

where $\mathbf{H}$ and $\mathbf{A}^v$ are constitutive matrixes. Other viscoelastic models can be drawn in the

similar procedure. Substitution eq. (3) into equilibrium equation,

$$-\rho\partial_t^2\mathbf{s} = \nabla\cdot\mathbf{T}, \tag{4}$$

Then the wave equation of viscoelastic media in frequency domain is given by

$$-\rho\omega^2\mathbf{s} = \nabla\cdot\left[\mathbf{H}:\frac{1}{2}\left(\nabla\mathbf{s}+(\nabla\mathbf{s})^T\right)\right]+\nabla\cdot\left[\mathbf{A}^v:\bar{\varphi}_{vl}\frac{1}{2}\left(\nabla\mathbf{s}+(\nabla\mathbf{s})^T\right)\right], \tag{5}$$

The second term of the right part of eq. (5) implies the viscosity of viscoelastic media.

2.2 Second-order M-PML formulations in viscoelastic media

For two-dimensional case, supposing vector **n** represents the normal vector of the interface between the absorbing regions and the regular region (Figure 1). The parallel direction of the boundary is represented as **m** in Figure 1, where the vectors **n** and **m** denote unit vectors $\vec{x}$ and $\vec{z}$ of 2D Cartesian coordinates in general. The gradient operator ∇ can be split in terms of components perpendicular and parallel to the interface

$$\boldsymbol{\nabla} = \mathbf{n}\partial_n + \boldsymbol{\nabla}^{//} = \mathbf{n}\partial_n + \mathbf{m}\partial_m, \tag{6}$$

where $\partial_n = \mathbf{n}\cdot\boldsymbol{\nabla}$ and $\boldsymbol{\nabla}^{//} = (\mathbf{I}-\mathbf{nn})\cdot\boldsymbol{\nabla} = \mathbf{m}\partial_m$ with $\mathbf{I}$ the 2×2 identity tensor. The M-PML formulations can be derived by introducing new complex coordinates $\tilde{n}$ and $\tilde{m}$ (Meza-Fajardo and Papageorgiou, 2008; Ping et al., 2014a),

$$\tilde{n}(n) = n - \frac{i}{\omega}\int_0^n d(s)ds, \tag{7a}$$

$$\tilde{m} = m + \frac{1}{i\omega}p^{(m/n)}d(n)m, \tag{7b}$$

where $d(\xi)$ denotes the damping profile in the direction of **n**, $p^{(m/n)}$ is a constant for fine-tuning of the stability of the M-PML terminations. Therefore, the relation between the new and the regular coordinates can be expressed by

$$
\begin{aligned}
&\frac{\partial n}{\partial \tilde{n}} = \frac{i\omega}{i\omega + d(n)}, \\
&\frac{\partial}{\partial n}\left(\frac{\partial n}{\partial \tilde{n}}\right) = \frac{i\omega}{(i\omega + d(n))^2}\frac{\partial d(n)}{\partial n}, \\
&\frac{\partial}{\partial m}\left(\frac{\partial n}{\partial \tilde{n}}\right) = 0, \\
&\frac{\partial m}{\partial \tilde{m}} = \frac{i\omega}{i\omega + d(m)}, \\
&\frac{\partial}{\partial n}\left(\frac{\partial m}{\partial \tilde{m}}\right) = -\frac{i\omega}{(i\omega + d(m))^2}\, p^{(m/n)} d^{'}(n), \\
&\frac{\partial}{\partial m}\left(\frac{\partial m}{\partial \tilde{m}}\right) = 0,
\end{aligned}
\tag{8}
$$

where $d(n)$, the damping profile is equal to 0 in regular region and greater than 0 in PML.

Substitution eq. (6) into eq. (5), the wave equation in the new complex coordinates is given by

$$
\begin{aligned}
-\rho\omega^2\mathbf{s} = {} & \mathbf{n}\partial_{\tilde{n}} \cdot \left[\mathbf{H} : \frac{\mathbf{1}}{\mathbf{2}}\left((\mathbf{n}\partial_{\tilde{n}}\mathbf{s}) + (\mathbf{n}\partial_{\tilde{n}}\mathbf{s})^T\right)\right] + \mathbf{n}\partial_{\tilde{n}} \cdot \left[\mathbf{H} : \frac{\mathbf{1}}{\mathbf{2}}\left((\mathbf{m}\partial_{\tilde{m}}\mathbf{s}) + (\mathbf{m}\partial_{\tilde{m}}\mathbf{s})^T\right)\right] \\
& + \nabla^{//} \cdot \left[\mathbf{H} : \frac{\mathbf{1}}{\mathbf{2}}\left((\mathbf{n}\partial_{\tilde{n}}\mathbf{s}) + (\mathbf{n}\partial_{\tilde{n}}\mathbf{s})^T\right)\right] + \nabla^{//} \cdot \left[\mathbf{H} : \frac{\mathbf{1}}{\mathbf{2}}\left((\mathbf{m}\partial_{\tilde{m}}\mathbf{s}) + (\mathbf{m}\partial_{\tilde{m}}\mathbf{s})^T\right)\right] \\
& + \mathbf{n}\partial_{\tilde{n}} \cdot \left[\mathbf{A}^{\mathbf{v}} : \bar{\varphi}_{vl}\frac{\mathbf{1}}{\mathbf{2}}\left((\mathbf{n}\partial_{\tilde{n}}\mathbf{s}) + (\mathbf{n}\partial_{\tilde{n}}\mathbf{s})^T\right)\right] + \mathbf{n}\partial_{\tilde{n}} \cdot \left[\mathbf{A}^{\mathbf{v}} : \bar{\varphi}_{vl}\frac{\mathbf{1}}{\mathbf{2}}\left((\mathbf{m}\partial_{\tilde{m}}\mathbf{s}) + (\mathbf{m}\partial_{\tilde{m}}\mathbf{s})^T\right)\right] \\
& + \nabla^{//} \cdot \left[\mathbf{A}^{\mathbf{v}} : \bar{\varphi}_{vl}\frac{\mathbf{1}}{\mathbf{2}}\left((\mathbf{n}\partial_{\tilde{n}}\mathbf{s}) + (\mathbf{n}\partial_{\tilde{n}}\mathbf{s})^T\right)\right] + \nabla^{//} \cdot \left[\mathbf{A}^{\mathbf{v}} : \bar{\varphi}_{vl}\frac{\mathbf{1}}{\mathbf{2}}\left((\mathbf{m}\partial_{\tilde{m}}\mathbf{s}) + (\mathbf{m}\partial_{\tilde{m}}\mathbf{s})^T\right)\right],
\end{aligned}
\tag{9}
$$

where $\bar{\varphi}_{vl}(\omega)$ represents Fourier transform of $\varphi_{vl}(t)$. It needs to be noticed that the last four terms of right part of eq. (9), which imply the viscosity of viscoelastic media, are introduced complex coordinates as well. Taking into account of eq. (8), eq. (9) can be rewritten as

$$
\begin{aligned}
-\rho\omega^2\mathbf{s} = {} & \mathbf{n}\partial_n \cdot \left[\mathbf{H} : \frac{\mathbf{1}}{\mathbf{2}}\left((\mathbf{n}\partial_n\mathbf{s}) + (\mathbf{n}\partial_n\mathbf{s})^T\right)\right](\partial n/\partial\tilde{n})^2 \\
& + \mathbf{n} \cdot \left[\mathbf{H} : \frac{\mathbf{1}}{\mathbf{2}}\left((\mathbf{n}\partial_n\mathbf{s}) + (\mathbf{n}\partial_n\mathbf{s})^T\right)\right](\partial n/\partial\tilde{n})\partial_n(\partial n/\partial\tilde{n})
\end{aligned}
$$

$$
\begin{aligned}
&+\left\{\mathbf{n}\partial_n\cdot\left[\mathbf{H}:\frac{\mathbf{1}}{\mathbf{2}}\left(\left(\nabla''\mathbf{s}\right)+\left(\nabla''\mathbf{s}\right)^T\right)\right]\right.\\
&\left.+\nabla''\cdot\left[\mathbf{H}:\frac{\mathbf{1}}{\mathbf{2}}\left(\left(\mathbf{n}\partial_n\mathbf{s}\right)+\left(\mathbf{n}\partial_n\mathbf{s}\right)^T\right)\right]\right\}(\partial n/\partial\tilde{n})(\partial m/\partial\tilde{m})\\
&+\mathbf{n}\cdot\left[\mathbf{H}:\frac{\mathbf{1}}{\mathbf{2}}\left(\left(\nabla''\mathbf{s}\right)+\left(\nabla''\mathbf{s}\right)^T\right)\right](\partial n/\partial\tilde{n})\partial_n(\partial m/\partial\tilde{m})\\
&+\mathbf{m}\cdot\left[\mathbf{H}:\frac{\mathbf{1}}{\mathbf{2}}\left(\left(\mathbf{n}\partial_n\mathbf{s}\right)+\left(\mathbf{n}\partial_n\mathbf{s}\right)^T\right)\right](\partial m/\partial\tilde{m})\partial_m(\partial n/\partial\tilde{n})\\
&+\nabla''\cdot\left[\mathbf{H}:\frac{\mathbf{1}}{\mathbf{2}}\left(\left(\nabla''\mathbf{s}\right)+\left(\nabla''\mathbf{s}\right)^T\right)\right](\partial m/\partial\tilde{m})^2\\
&+\mathbf{m}\cdot\left[\mathbf{H}:\frac{\mathbf{1}}{\mathbf{2}}\left(\left(\nabla''\mathbf{s}\right)+\left(\nabla''\mathbf{s}\right)^T\right)\right](\partial m/\partial\tilde{m})\partial_m(\partial m/\partial\tilde{m}),\\
&+\mathbf{n}\partial_n\cdot\left[\mathbf{A}^{\mathbf{v}}:\bar{\varphi}_{vl}\frac{\mathbf{1}}{\mathbf{2}}\left(\left(\mathbf{n}\partial_n\mathbf{s}\right)+\left(\mathbf{n}\partial_n\mathbf{s}\right)^T\right)\right](\partial n/\partial\tilde{n})^2\\
&+\mathbf{n}\cdot\left[\mathbf{A}^{\mathbf{v}}:\bar{\varphi}_{vl}\frac{\mathbf{1}}{\mathbf{2}}\left(\left(\mathbf{n}\partial_n\mathbf{s}\right)+\left(\mathbf{n}\partial_n\mathbf{s}\right)^T\right)\right](\partial n/\partial\tilde{n})\partial_n(\partial n/\partial\tilde{n})\\
&+\left\{\mathbf{n}\partial_n\cdot\left[\mathbf{A}^{\mathbf{v}}:\bar{\varphi}_{vl}\frac{\mathbf{1}}{\mathbf{2}}\left(\left(\nabla''\mathbf{s}\right)+\left(\nabla''\mathbf{s}\right)^T\right)\right]\right.\\
&\left.+\nabla''\cdot\left[\mathbf{A}^{\mathbf{v}}:\bar{\varphi}_{vl}\frac{\mathbf{1}}{\mathbf{2}}\left(\left(\mathbf{n}\partial_n\mathbf{s}\right)+\left(\mathbf{n}\partial_n\mathbf{s}\right)^T\right)\right]\right\}(\partial n/\partial\tilde{n})(\partial m/\partial\tilde{m})\\
&+\mathbf{n}\cdot\left[\mathbf{A}^{\mathbf{v}}:\bar{\varphi}_{vl}\frac{\mathbf{1}}{\mathbf{2}}\left(\left(\nabla''\mathbf{s}\right)+\left(\nabla''\mathbf{s}\right)^T\right)\right](\partial n/\partial\tilde{n})\partial_n(\partial m/\partial\tilde{m})\\
&+\mathbf{m}\cdot\left[\mathbf{A}^{\mathbf{v}}:\bar{\varphi}_{vl}\frac{\mathbf{1}}{\mathbf{2}}\left(\left(\mathbf{n}\partial_n\mathbf{s}\right)+\left(\mathbf{n}\partial_n\mathbf{s}\right)^T\right)\right](\partial m/\partial\tilde{m})\partial_m(\partial n/\partial\tilde{n})\\
&+\nabla''\cdot\left[\mathbf{A}^{\mathbf{v}}:\bar{\varphi}_{vl}\frac{\mathbf{1}}{\mathbf{2}}\left(\left(\nabla''\mathbf{s}\right)+\left(\nabla''\mathbf{s}\right)^T\right)\right](\partial m/\partial\tilde{m})^2,
\end{aligned}
\tag{10}
$$

Compared with Ping et al. (2014a), it is obvious that eq. (10) just contains seven more terms related to relaxation functions, which must be kept in PML formulation to keep physical consistency across the absorbing interface.

The displacement can be split into five parts as to obtain the split viscoelastic wave equations for M-PML in the frequency domain.

$$-\rho\omega^2\mathbf{s^1} = \mathbf{n}\partial_n \cdot \left[\mathbf{H} : \frac{\mathbf{1}}{\mathbf{2}}\left(\left(\mathbf{n}\partial_n\mathbf{s}\right) + \left(\mathbf{n}\partial_n\mathbf{s}\right)^T\right)\right](\partial n / \partial\tilde{n})^2 + \mathbf{n}\partial_n \cdot \left[\mathbf{A^v} : \bar{\varphi}_{vl}\frac{\mathbf{1}}{\mathbf{2}}\left(\left(\mathbf{n}\partial_n\mathbf{s}\right) + \left(\mathbf{n}\partial_n\mathbf{s}\right)^T\right)\right](\partial n / \partial\tilde{n})^2, \tag{11a}$$

$$-\rho\omega^2\mathbf{s^2} = \mathbf{n} \cdot \left[\mathbf{H} : \frac{\mathbf{1}}{\mathbf{2}}\left(\left(\mathbf{n}\partial_n\mathbf{s}\right) + \left(\mathbf{n}\partial_n\mathbf{s}\right)^T\right)\right](\partial n / \partial\tilde{n})\partial_n(\partial n / \partial\tilde{n}) + \mathbf{n} \cdot \left[\mathbf{A^v} : \bar{\varphi}_{vl}\frac{\mathbf{1}}{\mathbf{2}}\left(\left(\mathbf{n}\partial_n\mathbf{s}\right) + \left(\mathbf{n}\partial_n\mathbf{s}\right)^T\right)\right](\partial n / \partial\tilde{n})\partial_n(\partial n / \partial\tilde{n}), \tag{11b}$$

$$\begin{aligned}-\rho\omega^2\mathbf{s^3} = &\left\{\mathbf{n}\partial_n \cdot \left[\mathbf{H} : \frac{\mathbf{1}}{\mathbf{2}}\left(\left(\nabla''\mathbf{s}\right) + \left(\nabla''\mathbf{s}\right)^T\right)\right]\right. \\ &\left. + \nabla'' \cdot \left[\mathbf{H} : \frac{\mathbf{1}}{\mathbf{2}}\left(\left(\mathbf{n}\partial_n\mathbf{s}\right) + \left(\mathbf{n}\partial_n\mathbf{s}\right)^T\right)\right]\right\}(\partial n / \partial\tilde{n})(\partial m / \partial\tilde{m}) \\ &+ \left\{\mathbf{n}\partial_n \cdot \left[\mathbf{A^v} : \bar{\varphi}_{vl}\frac{\mathbf{1}}{\mathbf{2}}\left(\left(\nabla''\mathbf{s}\right) + \left(\nabla''\mathbf{s}\right)^T\right)\right]\right. \\ &\left. + \nabla'' \cdot \left[\mathbf{A^v} : \bar{\varphi}_{vl}\frac{\mathbf{1}}{\mathbf{2}}\left(\left(\mathbf{n}\partial_n\mathbf{s}\right) + \left(\mathbf{n}\partial_n\mathbf{s}\right)^T\right)\right]\right\}(\partial n / \partial\tilde{n})(\partial m / \partial\tilde{m}),\end{aligned} \tag{11c}$$

$$-\rho\omega^2\mathbf{s}^4 = \nabla'' \cdot \left[\mathbf{H} : \frac{\mathbf{1}}{\mathbf{2}}\left(\left(\nabla''\mathbf{s}\right) + \left(\nabla''\mathbf{s}\right)^T\right)\right](\partial m / \partial\tilde{m})^2 + \nabla'' \cdot \left[\mathbf{A^v} : \bar{\varphi}_{vl}\frac{\mathbf{1}}{\mathbf{2}}\left(\left(\nabla''\mathbf{s}\right) + \left(\nabla''\mathbf{s}\right)^T\right)\right](\partial m / \partial\tilde{m})^2, \tag{11d}$$

$$-\rho\omega^2\mathbf{s^5} = \mathbf{n} \cdot \left[\mathbf{H} : \frac{\mathbf{1}}{\mathbf{2}}\left(\left(\nabla''\mathbf{s}\right) + \left(\nabla''\mathbf{s}\right)^T\right)\right](\partial n / \partial\tilde{n})\partial_n(\partial m / \partial\tilde{m}) + \mathbf{n} \cdot \left[\mathbf{A^v} : \bar{\varphi}_{vl}\frac{\mathbf{1}}{\mathbf{2}}\left(\left(\nabla''\mathbf{s}\right) + \left(\nabla''\mathbf{s}\right)^T\right)\right](\partial n / \partial\tilde{n})\partial_n(\partial m / \partial\tilde{m}), \tag{11e}$$

The weak form of the second-order M-PML formulations in viscoelastic wave equations can be obtained by multiplying eq. (11) with the test vector $\mathbf{w}$ and then converting back into the time domain.

$$\int_V \rho(\partial_t + d(n))^2 \mathbf{s}^1 \cdot \mathbf{w} d^2\mathbf{r} = -\int_V (\mathbf{n}\partial_n \mathbf{w}) : \mathbf{H} : \frac{\mathbf{1}}{\mathbf{2}}\left((\mathbf{n}\partial_n \mathbf{s}) + (\mathbf{n}\partial_n \mathbf{s})^T\right) d^2\mathbf{r}$$
$$+ \int_\Gamma (\mathbf{nw}) : \mathbf{H} : \frac{\mathbf{1}}{\mathbf{2}}\left((\mathbf{n}\partial_n \mathbf{s}) + (\mathbf{n}\partial_n \mathbf{s})^T\right) d\mathbf{r}$$
$$- \int_V (\mathbf{n}\partial_n \mathbf{w}) : \mathbf{A}^v : \left(\varphi_{vl} * \frac{\mathbf{1}}{\mathbf{2}}\left((\mathbf{n}\partial_n \mathbf{s}) + (\mathbf{n}\partial_n \mathbf{s})^T\right)\right) d^2\mathbf{r}$$
$$+ \int_\Gamma (\mathbf{nw}) : \mathbf{A}^v : \left(\varphi_{vl} * \frac{\mathbf{1}}{\mathbf{2}}\left((\mathbf{n}\partial_n \mathbf{s}) + (\mathbf{n}\partial_n \mathbf{s})^T\right)\right) d\mathbf{r}, \tag{12a}$$

$$\int_V \rho(\partial_t + d(n))^3 \mathbf{s}^2 \cdot \mathbf{w} d^2\mathbf{r} = -\int_V d'(n)\mathbf{nw} : \mathbf{H} : \frac{\mathbf{1}}{\mathbf{2}}\left((\mathbf{n}\partial_n \mathbf{s}) + (\mathbf{n}\partial_n \mathbf{s})^T\right) d^2\mathbf{r}$$
$$- \int_V d'(n)\mathbf{nw} : \mathbf{A}^v : \left(\varphi_{vl} * \frac{\mathbf{1}}{\mathbf{2}}\left((\mathbf{n}\partial_n \mathbf{s}) + (\mathbf{n}\partial_n \mathbf{s})^T\right)\right) d^2\mathbf{r}, \tag{12b}$$

$$\int_V \rho\left[\partial_t^2 + (d(m) + d(n))\partial_t + d(m)d(n)\right] \mathbf{s}^3 \cdot \mathbf{w} d^2\mathbf{r}$$
$$= -\int_V \left[(\mathbf{n}\partial_n \mathbf{w}) : \mathbf{H} : \frac{\mathbf{1}}{\mathbf{2}}\left((\nabla'' \mathbf{s}) + (\nabla'' \mathbf{s})^T\right)\right.$$
$$\left. + (\nabla'' \mathbf{w}) : \mathbf{H} : \frac{\mathbf{1}}{\mathbf{2}}\left((\mathbf{n}\partial_n \mathbf{s}) + (\mathbf{n}\partial_n \mathbf{s})^T\right)\right] d^2\mathbf{r}$$
$$+ \int_\Gamma (\mathbf{nw}) : \mathbf{H} : \frac{\mathbf{1}}{\mathbf{2}}\left((\nabla'' \mathbf{s}) + (\nabla'' \mathbf{s})^T\right) d\mathbf{r} \tag{12c}$$
$$- \int_V \left[(\mathbf{n}\partial_n \mathbf{w}) : \mathbf{A}^v : \left(\varphi_{vl} * \frac{\mathbf{1}}{\mathbf{2}}\left((\nabla'' \mathbf{s}) + (\nabla'' \mathbf{s})^T\right)\right)\right.$$
$$\left. + (\nabla'' \mathbf{w}) : \mathbf{A}^v : \left(\varphi_{vl} * \frac{\mathbf{1}}{\mathbf{2}}\left((\mathbf{n}\partial_n \mathbf{s}) + (\mathbf{n}\partial_n \mathbf{s})^T\right)\right)\right] d^2\mathbf{r}$$
$$+ \int_\Gamma (\mathbf{nw}) : \mathbf{A}^v : \left(\varphi_{vl} * \frac{\mathbf{1}}{\mathbf{2}}\left((\nabla'' \mathbf{s}) + (\nabla'' \mathbf{s})^T\right)\right) d\mathbf{r},$$

$$\int_V \rho(\partial_t + d(m))^2 \mathbf{s}^4 \cdot \mathbf{w} d^2\mathbf{r} = -\int_V (\nabla'' \mathbf{w}) : \mathbf{H} : \frac{\mathbf{1}}{\mathbf{2}}\left((\nabla'' \mathbf{s}) + (\nabla'' \mathbf{s})^T\right) d^2\mathbf{r}$$
$$- \int_V (\nabla'' \mathbf{w}) : \mathbf{A}^v : \left(\varphi_{vl} * \frac{\mathbf{1}}{\mathbf{2}}\left((\nabla'' \mathbf{s}) + (\nabla'' \mathbf{s})^T\right)\right) d^2\mathbf{r}, \tag{12d}$$

$$\int_V \rho(\partial_t + d(m))^2 (\partial_t + d(n)) \mathbf{s}^5 \cdot \mathbf{w} d^2\mathbf{r}$$
$$= -\int_V p^{(m/n)} d'(n)\mathbf{nw} : \mathbf{H} : \frac{\mathbf{1}}{\mathbf{2}}\left((\nabla'' \mathbf{s}) + (\nabla'' \mathbf{s})^T\right) d^2\mathbf{r} \tag{12e}$$
$$- \int_V p^{(m/n)} d'(n)\mathbf{nw} : \mathbf{A}^v : \left(\varphi_{vl} * \frac{\mathbf{1}}{\mathbf{2}}\left((\nabla'' \mathbf{s}) + (\nabla'' \mathbf{s})^T\right)\right) d^2\mathbf{r},$$

where $d(m) = p^{(m/n)} d(n)$, the boundary Γ denotes the boundary of the PML that is not in

contact with the regular region. The summation of the split displacements represents the real displacement in M-PML.

$$\mathbf{s} = \mathbf{s^1} + \mathbf{s}^2 + \mathbf{s}^3 + \mathbf{s}^4 + \mathbf{s}^5, \tag{13}$$

Eq. (12) can be solved in explicit time scheme. Considering eq. (2b), the general appearance of the convolution term is

$$\phi(t) = a\exp(-bt)\bar{u}(t) * g(t) = \int_0^t a\exp(-b\tau)g(t-\tau)d\tau, \tag{14}$$

where a and b are constants, the term g is the state field variable of analysis (e.g. the displacement $\mathbf{s}$, $\left(\left(\nabla'' \mathbf{s}\right) + \left(\nabla'' \mathbf{s}\right)^T\right)$, and $\left(\left(\mathbf{n}\partial_n \mathbf{s}\right) + \left(\mathbf{n}\partial_n \mathbf{s}\right)^T\right)$). The iteration algorithm of eq. (14) can be derived from the convolution approach in C-PML (Matzen, 2011),

$$\psi^n = \zeta^{1/2} s^{n-1} + \exp(-b\Delta t)\psi^{n-1}, \tag{15a}$$

$$\phi^n = \zeta^0 s^n + \psi^n, \tag{15b}$$

where ζ^0 and $\zeta^{1/2}$ are given by

$$\zeta^0 = \frac{a}{b}\left[1 - \exp(-b\Delta t/2)\right], \tag{16a}$$

$$\zeta^{k+1/2} = \frac{a}{b}\left[1 - \exp(-b\Delta t)\right]\exp(-b(k+1/2)\Delta t), \tag{16b}$$

which are more accurate than the authors' proposed method (Ping et al. 2014b).

Actually, we note that these second-order M-PML formulations could be written for different second-order numerical schemes, e.g. the SEM, FEM and FDM. The second-order M-PML formulations (eq. (12)) for viscoelastic media can degrade into the M-PML for elastic media, when the properties of media change to elastic. The treatment of the corner regions for the second-order M-PML for viscoelastic wave equations is similar to that of the second-order M-PML for elastic wave equations (Ping et al., 2014a).

2.3 Formulations of second-order C-PML in viscoelastic media

The transformations resulting from the coordinate stretching approach in C-PML formulations (Figure 1, with no damping in direction of **m**) can be written as (Matzen, 2011)

$$\tilde{n}(n,\omega)=\int_0^n\left(\kappa_n(\varsigma)+\frac{d_n(\varsigma)}{\alpha_n(\varsigma)+j\omega}\right)d\varsigma=\int_0^n r_n(\varsigma,\omega)d\varsigma\,, \tag{17}$$

where $d_n \geq 0$ is a coordinate-wise real function and controls the attenuation of the propagating waves. The coordinate-wise real functions $\kappa_n \geq 1$ and $\alpha_n \geq 0$ serve to enhance attenuation of evanescent and near-grazing waves. Consideration damping waves in the direction of **m** in corner regions, the gradient operator becomes

$$\tilde{\nabla}=\left(\frac{\partial}{\partial\tilde{n}},\frac{\partial}{\partial\tilde{m}}\right)^T=\left(\frac{1}{r_n}\frac{\partial}{\partial n},\frac{1}{r_m}\frac{\partial}{\partial m}\right)^T, \tag{18}$$

where r_m and r_n are the damping functions (see Figure 2). Substitution eq. (18) to eq. (5),

$$\nabla\cdot\mathbf{T}'=-\omega^2\rho'\mathbf{s}, \tag{19a}$$

$$\mathbf{T}_V{}'=\mathbf{H}'\partial\mathbf{s}+\sum_{l=1}^{Lv}\bar{\varphi}_{vl}\mathbf{A}^{v'}\partial\mathbf{s}\,, \tag{19b}$$

where $\rho'=\rho r_m r_n$ and

$$\mathbf{T}'=r_m r_n\begin{pmatrix}\frac{1}{r_n} & \\ & \frac{1}{r_m}\end{pmatrix}\cdot\mathbf{T}\,, \tag{20}$$

The detailed version of eq. (19b) can also be written as

$$\begin{pmatrix} T_{11}^{'} \\ T_{22}^{'} \\ \frac{1}{2}\left(T_{21}^{'}+T_{12}^{'}\right) \\ \frac{1}{2}\left(T_{21}^{'}-T_{12}^{'}\right) \end{pmatrix} = \begin{pmatrix} H_{11}^{'} & H_{12} & & \\ H_{12} & H_{22}^{'} & & \\ & & H_{66}^{'} & H_{66}^{''} \\ & & H_{66}^{''} & H_{66}^{'''} \end{pmatrix} \begin{pmatrix} \frac{\partial}{\partial n} & 0 \\ 0 & \frac{\partial}{\partial m} \\ \frac{\partial}{\partial m} & \frac{\partial}{\partial n} \\ \frac{\partial}{\partial m} & -\frac{\partial}{\partial n} \end{pmatrix} \begin{pmatrix} s_1 \\ s_2 \end{pmatrix}$$

$$+\sum_{l=1}^{Lv} \bar{\varphi}_{vl} \begin{pmatrix} A^{v}_{11}{}^{'} & A^{v}_{12} & & \\ A^{v}_{12} & A^{v}_{22}{}^{'} & & \\ & & A^{v}_{66}{}^{'} & A^{v}_{66}{}^{''} \\ & & A^{v}_{66}{}^{''} & A^{v}_{66}{}^{'''} \end{pmatrix} \begin{pmatrix} \frac{\partial}{\partial n} & 0 \\ 0 & \frac{\partial}{\partial m} \\ \frac{\partial}{\partial m} & \frac{\partial}{\partial n} \\ \frac{\partial}{\partial m} & -\frac{\partial}{\partial n} \end{pmatrix} \begin{pmatrix} s_1 \\ s_2 \end{pmatrix}, \tag{21}$$

where

$$\begin{aligned} &H_{11}^{'} = r_m H_{11} / r_n, \qquad H_{22}^{'} = r_n H_{22} / r_m, \\ &A^{v}_{11}{}^{'} = r_m A^{v}_{11} / r_n, \qquad A^{v}_{22}{}^{'} = r_n A^{v}_{22} / r_m, \\ &H_{66}^{'} = \frac{H_{66}}{4}\left(\frac{r_n}{r_m}+\frac{r_m}{r_n}+2\right), \qquad A^{v}_{66}{}^{'} = \frac{A^{v}_{66}}{4}\left(\frac{r_n}{r_m}+\frac{r_m}{r_n}+2\right), \\ &H_{66}^{''} = \frac{H_{66}}{4}\left(\frac{r_n}{r_m}-\frac{r_m}{r_n}\right), \qquad A^{v}_{66}{}^{''} = \frac{A^{v}_{66}}{4}\left(\frac{r_n}{r_m}-\frac{r_m}{r_n}\right), \\ &H_{66}^{'''} = \frac{H_{66}}{4}\left(\frac{r_n}{r_m}+\frac{r_m}{r_n}-2\right), \qquad A^{v}_{66}{}^{'''} = \frac{A^{v}_{66}}{4}\left(\frac{r_n}{r_m}+\frac{r_m}{r_n}-2\right), \end{aligned} \tag{22}$$

We can identify the kinematic operator as

$$\partial = \begin{pmatrix} \frac{\partial}{\partial n} & 0 \\ 0 & \frac{\partial}{\partial m} \\ \frac{\partial}{\partial m} & \frac{\partial}{\partial n} \\ \frac{\partial}{\partial m} & -\frac{\partial}{\partial n} \end{pmatrix}. \tag{23}$$

In order to construct the time-domain formulations, we split the constitutive matrix into a non-stretched part and two stretched parts, respectively (Matzen, 2011),

$$\begin{aligned}
\mathbf{H}' &= \underbrace{\mathbf{D}_0 \otimes \mathbf{H}}_{\mathbf{H}_0} + \frac{r_1}{r_2}\underbrace{\mathbf{D}_1 \otimes \mathbf{H}}_{\mathbf{H}_1} + \frac{r_2}{r_1}\underbrace{\mathbf{D}_2 \otimes \mathbf{H}}_{\mathbf{H}_2}, \\
\mathbf{A}^{\nu\prime} &= \underbrace{\mathbf{D}_0 \otimes \mathbf{A}^{\nu}}_{\mathbf{A}^{\nu}{}_0} + \frac{r_1}{r_2}\underbrace{\mathbf{D}_1 \otimes \mathbf{A}^{\nu}}_{\mathbf{A}^{\nu}{}_1} + \frac{r_2}{r_1}\underbrace{\mathbf{D}_2 \otimes \mathbf{A}^{\nu}}_{\mathbf{A}^{\nu}{}_2},
\end{aligned} \tag{24}$$

The matrix operators $\mathbf{D}_0$, $\mathbf{D}_1$ and $\mathbf{D}_2$ can be deduced from eq. (22) and eq. (24) as

$$\mathbf{D}_0 = \begin{pmatrix} 0 & 1 & 0 & 0 \\ 1 & 0 & 0 & 0 \\ 0 & 0 & \frac{1}{2} & 0 \\ 0 & 0 & 0 & -\frac{1}{2} \end{pmatrix}, \quad \mathbf{D}_1 = \begin{pmatrix} 0 & 0 & 0 & 0 \\ 0 & 1 & 0 & 0 \\ 0 & 0 & \frac{1}{4} & \frac{1}{4} \\ 0 & 0 & \frac{1}{4} & \frac{1}{4} \end{pmatrix}, \quad \mathbf{D}_1 = \begin{pmatrix} 1 & 0 & 0 & 0 \\ 0 & 0 & 0 & 0 \\ 0 & 0 & \frac{1}{4} & -\frac{1}{4} \\ 0 & 0 & -\frac{1}{4} & \frac{1}{4} \end{pmatrix}, \tag{25}$$

Applying the inverse Fourier transform to eq. (19), the wave equations in viscoelastic media can be written as

$$\nabla \cdot \mathbf{T}' = \rho \Upsilon_0(t)\mathbf{s}, \tag{26a}$$

$$\mathbf{T}_{\mathrm{V}}{}' = \mathbf{H}'\partial\mathbf{s} + \sum_{l=1}^{Lv} \varphi_{vl} * \mathbf{A}^{\nu\prime}\partial\mathbf{s}, \tag{26b}$$

where

$$\begin{aligned}
\mathbf{H}' &= \mathbf{H}_0 + \Upsilon_1(t)\mathbf{H}_1 + \Upsilon_2(t)\mathbf{H}_2, \\
\mathbf{A}^{\nu\prime} &= \mathbf{A}^{\nu}{}_0 + \Upsilon_1(t)\mathbf{A}^{\nu}{}_1 + \Upsilon_2(t)\mathbf{A}^{\nu}{}_2,
\end{aligned} \tag{27}$$

the operator $\Upsilon_0(t)$, $\Upsilon_1(t)$ and $\Upsilon_2(t)$ are the inverse Fourier transform of $-\omega^2 r_n r_m$, r_n / r_m and r_m / r_n, the details of which are referred to Matzen (2011).

The equivalent integral weak form of eq. (26) with free-surface boundary condition can be deduced as the following

$$\int_{\Omega} \rho(\delta\mathbf{s})^T \Upsilon_0 \mathbf{s} d\Omega + \int_{\Omega} (\partial(\delta\mathbf{s}))^T \mathbf{T}'_{\nu} d\Omega = 0, \tag{28}$$

By simplifying eq. (28) and discretization of the displacements inside an element, the second-order C-PML formulations for SEM in viscoelastic media can be represented as

$$\mathbf{M}\ddot{\mathbf{s}} + \mathbf{Z}\dot{\mathbf{s}} + \mathbf{K}\mathbf{s} + \mathbf{h} + \mathbf{g} + \mathbf{g}_{visco} = \mathbf{f}_{visco}, \tag{29}$$

where the system matrices **M**, **Z**, and **K** are assembled from their element-level matrices $\mathbf{M}^{\mathbf{e}}$, $\mathbf{Z}^{\mathbf{e}}$, and $\mathbf{K}^{\mathbf{e}}$, respectively,

$$\mathbf{M}^e = \int_{\Omega^e} \rho P_0 \mathbf{N}^T \mathbf{N} d\Omega, \tag{30a}$$

$$\mathbf{Z}^e = \int_{\Omega^e} \rho P_1 \mathbf{N}^T \mathbf{N} d\Omega, \tag{30b}$$

$$\mathbf{K}^e = \int_{\Omega^e} \rho P_2 \mathbf{N}^T \mathbf{N} d\Omega + \int_{\Omega^e} \mathbf{B}^T \left(\mathbf{H}_0 + \frac{\kappa_n}{\kappa_m} \mathbf{H}_1 + \frac{\kappa_m}{\kappa_n} \mathbf{H}_2 \right) \mathbf{B} d\Omega, \tag{30c}$$

Here, **N** is the interpolation matrix and $\mathbf{B} = \partial \mathbf{N}$ denotes the strain-displacement matrix. In particular, compared with the second-order C-PML in elastic media (Matzen, 2011), two more vectors $\mathbf{g}_{\text{visco}}$ and $\mathbf{f}_{\text{visco}}$ need to be calculate in eq. (29), besides the convolution vectors **h** and **g**,

$$\mathbf{h}^e = \int_{\Omega^e} \rho \mathbf{N}^T \mathbf{N} \left[{\alpha_n}^2 P_{3,1} \exp(-\alpha_n t) \bar{u}(t) + {\alpha_m}^2 P_{3,2} \exp(-\alpha_m t) \bar{u}(t) \right] * \mathbf{s}^e d\Omega, \tag{31a}$$

$$\begin{aligned} \mathbf{g}^e = & \int_{\Omega^e} \mathbf{B}^T \left[\mathbf{H_1 B} \frac{{d_n}^2}{P_{3,1}} \exp(-\alpha_n t) \bar{u}(t) + \mathbf{H_2 B} \frac{{d_m}^2}{P_{3,2}} \exp(-\alpha_m t) \bar{u}(t) \right] * \mathbf{s}^e d\Omega \\ & - \int_{\Omega^e} \mathbf{B}^T \left[\mathbf{H_1 B} P_{4,2} \exp(-(d_m + \kappa_m \alpha_m) t / \kappa_m) \bar{u}(t) \right. \\ & \left. + \mathbf{H_2 B} P_{4,1} \exp(-(d_n + \kappa_n \alpha_n) t / \kappa_n) \bar{u}(t) \right] * \mathbf{s}^e d\Omega, \end{aligned} \tag{31b}$$

$$\begin{aligned} {\mathbf{g}_{visco}}^e = & \int_{\Omega^e} \mathbf{B}^T \left[\mathbf{A_1 B} \sum_{l=1}^{Lv} \varphi_{vl}(t) * \frac{{d_n}^2}{P_{3,1}} \exp(-\alpha_n t) \bar{u}(t) \right. \\ & \left. + \mathbf{A_2 B} \sum_{l=1}^{Lv} \varphi_{vl}(t) * \frac{{d_m}^2}{P_{3,2}} \exp(-\alpha_m t) \bar{u}(t) \right] * \mathbf{s}^e d\Omega \\ & - \int_{\Omega^e} \mathbf{B}^T \left[\mathbf{A_1 B} \sum_{l=1}^{Lv} \varphi_{vl}(t) * P_{4,2} \exp(-(d_m + \kappa_m \alpha_m) t / \kappa_m) \bar{u}(t) \right. \\ & \left. + \mathbf{A_2 B} \sum_{l=1}^{Lv} \varphi_{vl}(t) * P_{4,1} \exp(-(d_n + \kappa_n \alpha_n) t / \kappa_n) \bar{u}(t) \right] * \mathbf{s}^e d\Omega, \end{aligned} \tag{31c}$$

$${\mathbf{f}_{visco}}^e = \int_{\Omega^e} \mathbf{B}^T \left(\mathbf{A}_0 + \frac{\kappa_n}{\kappa_m} \mathbf{A}_1 + \frac{\kappa_m}{\kappa_n} \mathbf{A}_2 \right) \mathbf{B} \sum_{l=1}^{Lv} \varphi_{vl} * \mathbf{s}^e d\Omega, \tag{31d}$$

where, the computation of $\mathbf{h}^{\mathrm{e}}$, $\mathbf{g}^{\mathrm{e}}$ and $\mathbf{f}^{\mathrm{e}}$ are the same as in the second-order elastic C-PML. While, it is crucial to calculate the convolution terms in vectors ${\mathbf{g}_{visco}}^{\mathrm{e}}$ and ${\mathbf{f}_{visco}}^{\mathrm{e}}$ for a uniform

physical consistency in the computational domain. In eq. (30) and eq. (31), $P_{0,}P_1$, $P_2, P_{3,\mathrm{i}}$ and $P_{4,\mathrm{i}}$ (i=1, 2) are the spatially varying functions (Matzen, 2011). The critical process of the second-order C-PML in viscoelastic media is to handle the secondary convolution terms in eq. (31c). Substituting eq. (2b) into eq. (31c), take the first term of right hand of eq. (31c) for example,

$$\begin{aligned}&\sum_{l=1}^{Lv}\varphi_{vl}(t)*\frac{d_n^{\,2}}{P_{3,1}}\exp(-\alpha_n t)\bar{u}(t)*\mathbf{s}^e\\&\quad=\frac{d_n^{\,2}}{P_{3,1}}\sum_{l=1}^{Lv}\frac{1}{Lv\cdot\tau_{\sigma l}^{(v)}}(1-\frac{\tau_{\varepsilon l}^{(v)}}{\tau_{\sigma l}^{(v)}})\exp(-t/\sigma_{\sigma l}^{(v)})*\exp(-\alpha_n t)\bar{u}(t)*\mathbf{s}^e,\end{aligned}\tag{32}$$

where,

$$\begin{aligned}&\exp(-t/\sigma_{\sigma l}^{(v)})*\exp(-\alpha_n t)\bar{u}(t)\\&\quad=\int\exp(-\tau/\sigma_{\sigma l}^{(v)})\exp(-\alpha_n(t-\tau))\bar{u}(t-\tau)d\tau\\&\quad=\int_0^t\exp(-\alpha_n t+(\alpha_n-1/\sigma_{\sigma l}^{(v)})\tau)d\tau\\&\quad=\frac{1}{\alpha_n-1/\sigma_{\sigma l}^{(v)}}[\exp(-1/\sigma_{\sigma l}^{(v)}t)-\exp(-\alpha_n t)],\end{aligned}\tag{33}$$

After substituting eqs. (32) and (33) into eq. (31), the first term of the vector $\mathbf{g}_{visco}^{\mathrm{e}}$ can be deduced,

$$\begin{aligned}&\int_{\Omega^e}\mathbf{B}^T[\mathbf{A}_1\mathbf{B}\sum_{l=1}^{Lv}\varphi_{vl}(t)*\frac{d_n^{\,2}}{P_{3,1}}\exp(-\alpha_n t)\bar{u}(t)*\mathbf{s}^e]d\Omega\\&=\int_{\Omega^e}\mathbf{B}^T[\mathbf{A}_1\mathbf{B}\frac{d_n^{\,2}}{P_{3,1}}\sum_{l=1}^{Lv}\frac{1}{Lv\cdot\tau_{\sigma l}^{(v)}}(1-\frac{\tau_{\varepsilon l}^{(v)}}{\tau_{\sigma l}^{(v)}})\frac{1}{\alpha_n-1/\sigma_{\sigma l}^{(v)}}[\exp(-1/\sigma_{\sigma l}^{(v)}t)-\exp(-\alpha_n t)]*\mathbf{s}^e d\Omega,\end{aligned}\tag{34}$$

Eq. (34) can be calculated the same as the vectors $\mathbf{h}^{\mathrm{e}}$ and $\mathbf{g}^{\mathrm{e}}$. So far, the vectors $\mathbf{g}_{visco}^{\mathrm{e}}$ and $\mathbf{f}_{visco}^{\mathrm{e}}$ related to the viscosity of the media can be obtained as the convolution vectors $\mathbf{h}^{\mathrm{e}}$ and $\mathbf{g}^{\mathrm{e}}$.

Similar to the second-order C-PML for elastic media, the C-PML for viscoelastic media acts as forcing terms $\mathbf{g}_{visco}^{\mathrm{e}}$ and $\mathbf{f}_{visco}^{\mathrm{e}}$ that can be recursively updated, like the convolution

vectors $\mathbf{h}^e$ and $\mathbf{g}^e$. The treatment of convolution terms represents in eqs. (14) – (16).

3. NUMERICAL EXAMPLES

To illustrate the efficiency of the developed M-PML and C-PML in second-order viscoelastic wave equations which have never been discussed before, we simulate 2D wave propagation in P-SV polarization plane in viscoelastic media. We apply the SEM with a polynomial degree $N = 4$, chosen in each element. An isotropic model with high Poisson's ratio and two anisotropic models, which have been found to yield the computational instabilities easily (Meza-Fajardo & Papageorgiou, 2008; Ping et al., 2014a), are selected for numerical efficiency tests. A general Zener model is chosen by setting $L_1 = L_2 = 2$ in eq. (2). The material properties of the models are given in Tables 1 and 2, in which the attenuation parameters used by Carcione et al. (1988) and Martin and Komatitsh (2009). It has to be emphasized that the primary scope of this paper is merely to demonstrate the performance of M-PML and C-PML employed in the viscoelastic wave equations that recast as the second-order system with the single unknown displacement field. After numerical comparisons we will try to give a 'rule of thumb' for the choice of PMLs in the second-order wave equations in viscoelastic media.

The free surface conditions are imposed on the outer edges of the viscoelastic PML regions (Figure 3). The time step is 0.04 ms for case 1, 1ms for case 2 and 0.1 ms for case 3. The total duration of the simulation are 6 s for case 1, 100 s for case 2, and 3.8 s for case 3, respectively.

The damping profiles of the C-PML are chosen as follows (Matzen, 2011),

$$\kappa_x = 1 + \kappa_{\max,x}\left(\frac{x}{\delta}\right)^{n1}, \tag{35a}$$

$$d_x = d_{\max,x}\left(\frac{x}{\delta}\right)^{n1+n2}, \tag{35b}$$

$$\alpha_x = \alpha_{\max,x}\left(\frac{\delta - x}{\delta}\right)^{n3}, \tag{35c}$$

with $\alpha_{\max,x} = 2\pi f_\alpha$ and

$$d_{\max,x} = \frac{(1+n1+n2)c_p}{2\delta}\log_{10}\left(\frac{1}{R}\right), \tag{35d}$$

$$\kappa_{\max,x} = \frac{(1+n1)b_x}{2\delta}\log_{10}\left(\frac{1}{R}\right), \tag{35e}$$

Here, δ is the width of the PML region; x is the distance from the PML boundary associated with the damping direction. R_0 is the reflection coefficient at normal incidence (we choose $R_0=10^{-8}$ in all cases), b_x is a characteristic length of the domain. We choose the following damping profile parameters: n1=3, n2=1, n3=1 for case 1, n1=3, n2=2, n3=1 for case 2 and case 3, respectively. These parameters have been slightly changed to avoid singularities for $P_{4,i}$ and $1/P_{3,i}$ (i=1,2).

The damping profile for M-PML is chosen as the same as eq. (35b) for comparisons. In addition, we also set n1+n2=2 in all cases for M-PML computation,

$$d_x = d_{\max,x}\left(\frac{x}{\delta}\right)^{2}, \tag{36}$$

which is the classical 2nd-order damping function for PMLs.

Case 1

In this case, the efficiency of the developed M-PML and C-PML in second-order viscoelastic wave equations is validated in an isotropic viscoelastic medium with a high

Poisson's ratio of $\nu = 0.47$, in which the near-surface wavefields are complicated due to the intricate interactions of various waves with the free surface and will introduce difficulties to the absorption of PMLs (Zeng et al., 2011). For the SEM implementation, the model is discretized in 70×45 elements (dx=dz=1 m). A point source is vertically excited at (35.0 m, 0 m) in the x-z plane with the time function as a Ricker wavelet (central frequency is 40 Hz, and time shift is 0.04 s). The PML absorbing boundaries (Figure 3) in two vertical and bottom edges are set to span of 8 m. There are eight layers of spectral elements in PML regions, containing $8N+1=33$ GLL-grid points in damping direction. A receiver at (38.75 m, 0.0 m) records the horizontal and vertical displacements. The snapshots of horizontal (Figure 4) and vertical (Figure 5) displacements are shown for the viscoelastic M-PML with 2nd-order (eq. 36) and high-order (eq. 35b) damping profiles and the viscoelastic C-PML.

On the snapshots from 0.072 s to 0.16 s (Figures 4a-b and 5a-b), the P wave has entered the PML regions and no spurious reflections appear in regular region for all PMLs. At t=0.24 s, the S wave and surface waves have propagated into the PML regions and are also efficiently absorbed (Figures 4c-d and5c-d) for the M-PMLs and C-PML. Some tiny reflections for the M-PMLs (left and middle panels in Figures 4c-d and 5c-d) can be visible which prove again that they do not perfectly matched in theory (Dmitriev & Lisitsa, 2011). When the body and surface waves propagate outside the simulated model, most of the spurious reflections are suppressed (Figures 4c-d and 5c-d), for the M-PMLs and C-PML. At t=0.32 s, although there are some acceptable tiny reflections in the regular region, most of the incident energies in M-PMLs are attenuated immediately and sightless (left and middle panels of Figures 4d and 5d). Violation of the displacement threshold is not observed in the

M-PMLs and C-PML terminations (Figures 4e and 5e) during the modeling. To get more insight into the accuracy of both PML implementations, we show the differences (Figure 6) between the M-PMLs, C-PML and the reference computed with the same numerical scheme on a very large mesh with no absorbing boundaries. The errors for horizontal and vertical components are smaller in C-PML before 0.32 s but greater at late time simulation around 0.32 to 0.45 s. These reflections are acceptable and can be ignored in general.

All these phenomena can be also verified in the energy curves in regular region for the viscoelastic M-PMLs and C-PML (Figure 6). Instability is not observed in all energy curves. The artificial reflections of the M-PMLs exceed that of the C-PML at some time steps (Figure 6), which can be also observed by comparing the energy decay curves for the M-PMLs and C-PML around 0.25 to 0.55 s (Figure 7). Moreover, the reflection energy from the M-PML with high-order damping profile exceeds that of the M-PML with 2nd-order damping profile around 0.7 to 1.0 s. However, the reflection energy for the M-PML with high-order damping profile keeps the lowest in the three curves after 1.0 s (Figure 7). It demonstrates that in the simulation time the M-PML is more stable than the C-PML in this viscoelastic medium, even using the same damping profiles. The M-PML with 2nd-order damping profile shows an unstable trend after 1.5 s. Its energy curve upwarps slowly after 1.5 s and exceeds that of the C-PML around 5.5 s. Therefore, in an isotropic viscoelastic medium with higher Poisson's ratio, the M-PML with 2nd-order damping profile is not an optimal choice. It is worth mentioning that for the C-PML the weak oscillations appear and persist a long time in spite of that total energy decays very quickly. This illustrates that re-injections of energies in the regular region occur at long time for the C-PML scheme. This phenomenon can be reduced

by simple increasing the thickness of C-PML. In summary, the developed C-PML would be a sufficient choice compared with the M-PML in second-order viscoelastic wave equations for seismic wave simulations in an isotropic viscoelastic medium with a high Poisson's ratio.

Case 2

A particular orthotropic model which has been studied previously (Becache et. al, 2001; Meza-Fajardo & Papageorgiou, 2008; Ping et. al, 2014) is selected for tests of stability in long time simulation. Ping et al. (2014a) designed a stable M-PML for this particular medium with the second-order elastic wave equations. This model is further investigated for viscoelastic and anisotropic effects on the proposed second-order PMLs. We simulate the waves propagation in this anisotropic viscoelastic model (Table 2) consisting of 90×65 spectral elements in size of 24.92 m$\times$19.92 m. Three PML layers consisting of 61 grid points i.e. 15 spectral elements are designed to surround the model except for the free surface. The vertical point source was applied at (12.44m, 0m) with the time function of a Ricker wavelet (the central frequency and time shift are 0.9 Hz and 1 s, respectively). A receiver at (14.91 m, 0.0 m) records the displacements of wave propagation.

The snapshots at different times for the M-PMLs and the C-PML are displayed in Figures 8 and 9. The wavefields in the regular region spread and illuminate the body waves splitting (Figures 8a-8b and 9a-9b). At t=15 s, the wavefields have been propagated into the absorbing regions and absorbed efficiently both for M-PMLs and C-PML. But yet some insignificant reflections appear in case of the M-PMLs whether the 2nd-order damping profile or the higher-order damping profile is used (left and middle panels of Figures 8c and 9c, respectively). The unexpected energies can also be observed around 10 s to 33 s in Figure

10, which represents the time evolution of displacement differences subtracted from the recordings with PMLs and the reference without any absorbing boundaries (but with a very large mesh as described before). In addition the spurious waves appear at about t=30 s in the C-PML terminations (right panels of Figures 8d and 9d). The energy decay curves (Figure 11) show the same features: The total energy for C-PML grows up after 30 s, and the unexpected waves pollute the wavefields in the regular region. As noted again the unexpected waves will send spurious energy back into the regular region when the simulation runs for a long time. However, instabilities cannot be determinately identified for the M-PMLs (left and middle panels of Figures 8d-8e and 9d-9e). Different from case 1, the energy in the regular region for the M-PML with the 2nd-order damping profile decreases continuously in the whole simulation time, and the reflections from the boundaries do not exceed that of the M-PML with the high-order damping profile from 20 s to 93 s. It can be concluded that the M-PMLs have the superior stability than C-PML in this special anisotropic viscoelastic medium. For the whole simulation time, the absorbing efficiency of the M-PML with 2nd-order damping profile is slightly lower than that of the M-PML with high-order damping profile. Nevertheless, compared with the C-PML, the M-PML with 2nd-order damping profile works efficiently and stably in such a particular orthotropic viscoelastic model.

Case 3

The PMLs usually suffer from the late time instabilities in the numerical simulation for rather common materials (such as zinc) (e.g., Meza-Fajardo & Papageorgiou, 2008; Matzen, 2011; Ping et al., 2014a). These simulation instabilities may be likely to happen in coupled viscoelastic and anisotropic model when the second-order equations are used and need to be

investigated further. An anisotropic viscoelastic model (Case 3 in Table 2) is comprised of a 948 m×648 m regular region with 180-m-thick-PML layers in three absorbing regions (Figure 3). The excitation is applied by a vertical point force at (533.1 m, 0 m) which changes as a Ricker wavelet with 40 Hz central frequency and 0.05 s time shift, respectively. A receiver is placed at (633.0 m, 0 m).

The horizontal (Figure 12) and vertical (Figure 13) displacement snapshots are simulated for the M-PMLs with different orders of damping profiles, and C-PML, respectively. The wavefields in the regular region spread normally without instability appearing in the whole time simulation (Figures 12a and 13a). The incident wavefields are absorbed efficiently for the M-PMLs and C-PML (Figure 12b-12e and 13b-13e), although minor spurious reflections can be observed in the PML terminations (Figure 12b-12c and 13b-13c). Subtracting the records in models with the PMLs from those in the reference model without absorbing regions, the visible differences appear at around 0.3 s in Figure 14. The wavefields have totally propagated into absorbing regions at 0.4 s and no significant reflection energy appears in the regular region (Figures 12d and 13d). At t=3 s the incident wavefields are all damped out in the PML terminations (Figures 12e and 13e) and no instabilities are observed. We can identify these phenomena in the energy decay curves (Figure 15). In addition, the reflections in the M-PML with high-order damping profile exceed that of the M-PML with 2nd-order damping profile between 0.4 s to 2 s. The M-PMLs seem to maintain the similar stability for long time simulation. It is noticed that the energy curves for the M-PMLs do not exceed that of the C-PML almost in whole simulation time, indicating M-PMLs superior to the C-PML. These features can also be observed in Figure 14b where the error for C-PML exceeds those

of the M-PMLs after 0.4 s. To reduce the reflections from PML boundaries, the M-PML with 2nd-order damping profile is sufficient in this anisotropic viscoelastic medium.

Based upon the viscoelastic and anisotropic experiments, the firstly proposed second-order M-PML (especially one with 2nd-order damping profiles) may be a better choice for the simulations in second-order anisotropic viscoelastic wave equations.

4. DISCUSSION AND CONCLUSIONS

We have presented the M-PML and C-PML formulations for FEM and SEM simulations based upon the second-order viscoelastic seismic wave equations with displacements as the only unknown that have never been discussed before, where two or more viscoelastic standard linear solid (SLS) damping mechanisms are used. The PMLs without additional auxiliary differential equations, allow us to easily use the second-order SEM and FEM with more economical computational consumption, as well as without entire reconstruction of the existed codes.

After the numerical comparison of the C-PML, the M-PML with high-order damping profile, and the M-PML with 2nd-order damping profile, we can conclude that the second-order M-PML is more stable than the second-order C-PML even in viscoelastic media. However, for an isotropic viscoelastic medium with high Poisson's ratio, the C-PML would be sufficient for long time simulation because of its weak reflections and sufficient stability compared with the M-PML with 2nd-order damping profile. Furthermore the M-PML with high-order damping profile has a superior stability in long time simulation in an isotropic viscoelastic medium with high Poisson's ratio than the M-PML with 2nd-order damping

profile. In anisotropic viscoelastic media, the C-PML is likely to suffer from instability, the M-PML with 2nd-order damping profile will be a better choice for its superior stability and more weak reflections than the M-PML with high-order damping profile.

It is actually straightforward to derive the M-PML and C-PML in viscoelastic media and this decomposition has already been addressed by other authors as Carcione (2015) in first-order equations. We firstly present this decomposition to derive the PMLs in second-order viscoelastic wave equations, in order to obtain a uniform implementation of PMLs with physical consistency in computational domain, which can be applied directly to the existed second-order system codes with acceptable modifications. The established formulations are based upon the constitutional relation of viscoelastic media, and hence can be straightforwardly implemented in 3D seismic wave propagation. Without additional auxiliary differential equations and additional variables, the consumptions of memories and time do not significantly increase in viscoelastic PML formulations. In parallel computing, these differences will be reduced further. By application of these upscale PMLs, the second-order viscoelastic seismic wave modeling techniques, e.g. SEM and FEM, can handle more complex and realistic material systems.

Acknowledgment

Gratitude is expressed for the financial supports from the National Natural Science Foundation of China (NSFC) (41304077, 41374079), the National Basic Research Program of China (2013CB733203), the China Postdoctoral Foundation (2016M590734) and Hubei Subsurface Multi–scale Imaging Key Laboratory (SMIL).

References

Abarbanel, S. & Gottlieb, D., 1998. On the construction and analysis of absorbing layer in CEM, *Appl. Numer. Math.*, 27, 331–340.

Appelö, D. & Kreiss, G., 2005. A new absorbing layer for elastic waves, *J. Comput. Phys.*, 215, 642–660.

Basu, U. & Chopra, A.K., 2004. Perfectly matched layers for transient elastodynamics of unbounded domains, *Int. J. Numer. Methods Eng.*, 59, 1039–1074.

Bécache, E., Fauqueux, S., & Joly, P., 2001. Stability of perfectly matched layers, group velocities and anisotropic waves. *Rapport de recherche n°4304, Thème 4, Simulation et optimisation de systèmes complexes, Projet Ondes.* 1-35.

Bécache, E., Ezziani, A. & Joly, P., 2004. A mixed finite element approach for viscoelastic wave propagation, *Computational Geosciences*, 8, 255–299.

Bérenger, J.P., 1994. A perfectly matched layer for the absorption of electromagnetic waves, *J. Comput. Phys.*, 114, 185–200.

Bérenger, J.P., 2002. Numerical Reflection from FDTD-PMLs: a comparison of the split PML with the unsplit and CFS PMLs, *IEEE Trans. Antennas Propag.*, 50, 258–265.

Carcione, J.M., 1990. Wave propagation in anisotropic linear viscoelastic media: theory and simulated wavefields, *Geophys. J. Int.*, 101, 739-750.

Carcione, J.M., 2015. *Wave fields in real media: Wave propagation in anisotropic, anelastic, porous and electromagnetic media*, 3nd edn, pp. 222-227, Pergamon Press.

Carcione, J.M., Kosloff, D. & Kosloff, R., 1988. Wave propagation simulation in a linear viscoelastic medium, *Geophys. J. Int.*, 95, 597–611.

Chew, W.C. & Liu, Q.H., 1996. Perfectly matched layers for elastodynamics: a new absorbing boundary condition, *J. Comput. Acoust.*, 4, 341–359.

Collino, F. & Monk, P.B., 1998. Optimizing the perfectly matched layer, *Comput. Methods. Appl. Mech. Eng.*, 164, 157–171.

Collino, F. & Tsogka, C., 2001. Application of the perfectly matched layer absorbing layer model to the linear elastodynamic problem in anisotropic heterogeneous media, *Geophysics*, 66, 294–307.

Dmitriev, M.N. & Lisitsa, V.V., 2011. Application of M-PML Reflectionless Boundary Conditions to the Numerical Simulation of Wave Propagation in Anisotropic Media, Part I: Reflectivity., *Sib. Zh. Vych. Mat.,* 14, 333–344.

Dmitriev, M.N. & Lisitsa, V.V., 2012. Application of M-PML Reflectionless Boundary Conditions to the Numerical Simulation of Wave Propagation in Anisotropic Media, Part II: Stability, *Sib. Zh. Vych. Mat.,* 15, 45–55.

Du Q.Z. & Yang H.Z., 2003. Finite-element methods for viscoelastic and azimuthally anisotropic media, *Acta Physica Sinica*, 52, 2010–2014 (in Chinese with English abstract).

Duru, K., 2014. A perfectly matched layer for the time-dependent wave equation inheterogeneous and layered media, *Journal of Computational Physics,* 257, 757-781.

Duru, K. & Kreiss, G., 2012. A well-posed and discretely stable perfectly matched layer for elastic wave equations in second order formulation, *Commun. Comput. Phys.*, 11, 1643–1672.

Fathi, A., Poursartip, B. & Kallivokas, L.F., 2015. Time-domain hybrid formulations for wave

simulations in three-dimensional PML-truncated heterogeneous media, *Int. J. Numer. Methods Eng.*, 101, 165-198.

Feng, N. & Li, J., 2013. Novel and efficient FDTD implementation of higher order perfectly matched layer based on ADE method, *J. Comput. Phys.*, 232, 318–326.

Festa, G. & Nielsen, S., 2003. PML Absorbing Boundaries, *Bull. Seismol. Soc. Am.*, 93, 891–903.

Festa, G. & Vilotte, J.P., 2005. The Newmark scheme as velocity-stress time-staggering: an efficient PML implementation for spectral-element simulations of elastodynamics, *Geophys. J. Int.*, 161, 789–812.

Festa, G., Delavaud, E. & Vilotte, J.P., 2005. Interaction between surface waves and absorbing boundaries for wave propagation in geological basins: 2D numerical simulations, *Geophys. Res. Lett. 32*, L20306, doi: 10. 1029/2005GL024091.

Gao, Y., Zhang, J. & Yao., Z., 2015. Unsplit complex frequency shifted perfectly matched layer for second-order wave equation using auxiliary differential equations, *J. Acoust. Soc. Am.*, 138, 551-557.

Gedney, S.D., 1996. An anisotropic perfectly matched layer absorbing medium for the truncation of FDTD lattices, *IEEE Trans. Antennas Propag.*, 44, 1630–1639.

Gedney, S.D. & Zhao, B., 2010. An auxiliary differential equation formulation for the complex-frequency shifted PML, *IEEE Trans. Antennas Propag.*, 58, 838–847.

Halpern, L., Petit-Bergez, S. & Rauch, J., 2011. The Analysis of Matched Layers, *Confluentes Mathematici*, 3, 159–236.

Hastings, F.D., Schneider, J.B. & Broschat, S.L., 1996. Application of the perfectly matched

layer (PML) absorbing boundary condition to elastic wave propagation, *J. Acoust. Soc. Am.*, 100, 3061–3069.

Hesthaven, J.S., 1998. On the analysis and construction of perfectly matched layers for the linearized Euler equations, *J. Comput. Phys.*, 142, 129–147

Hu, F.Q., 1996. On absorbing boundary conditions for linearized Euler equations by a perfectly matched layer, *J. Comput. Phys.*, 129, 201–2019.

Komatitsch, D. & Martin, R., 2007. An unsplit convolutional perfectly matched layer improved at grazing incidence for the seismic wave equation, *Geophysics*, 72, SM155–SM167.

Kreiss, G., and Duru, K., 2013. Discrete stability of perfectly matched layers for anisotropic wave equations in first and second order formulation, *Bit Numer Math*, 53, 641-663.

Kuzuoglu, M. & Mittra, R., 1996. Frequency dependence of the constitutive parameters of causal perfectly matched anisotropic absorbers, *IEEE, Microw. and Guided Wave Lett.*, 6, 447–449.

Li, Y.F. & Matar, O.B., 2010. Convolutional perfectly matched layer for elastic second-order wave equation, *J. Acoust. Soc. Am.*, 127, 1318–1327.

Martin, R., Komatitsch, D. & Ezziani, A., 2008. An unsplit convolutional perfectly matched layer improved at grazing incidence for seismic wave equation in poroelastic media, Geophysics, 73, T51–T61.

Martin, R. & Komatitsch, D., 2009. An unsplit convolutional perfectly matched layer technique improved at grazing incidence for the viscoelastic wave equation, *Geophys. J. Int.*, 179, 333–344.

Martin, R., Komatitsch, D. & Gedney, S.D., 2009. A Variational Formulation of a Stabilized Unsplit Convolutional Perfectly Matched Layer for The Isotropicor Anisotropic Seismic Wave Equation, *Comput. Modeling Engrg. Sci*., 1131, 1-32.

Martin, R., Komatitsch, D., Gedney, S.D. & Bruthiaux, E., 2010. A high-order time and space formulation of the unsplit perfectly matched layer for the seismic wave equation using Auxiliary Differential Equations (ADE-PML), *Comput. Modeling Engrg. Sci*., 56, 17-41.

Matzen, R., 2011. An efficient finite element time-domain formulation for the elastic second-order wave equation: A non-split complex frequency shifted convoltional PML, *Int. J. Numer. Meth. Eng.*, 88, 951–973.

Meza-Fajardo, K.C. & Papageogiou, A.S., 2008. A nonconvolutional, split-field, perfectly matched layer for wave propagation in isotropic and anisotropic elastic media: stability analysis, *Bull. Seismol. Soc. Am.*, 98, 1811–1836.

Meza-Fajardo, K.C. & Papageogiou, A.S., 2010. On the stability of a non-convolutional perfectly matched layer for isotropic elastic media, *Soil Dynam. Earthquake Eng.*, 30, 68–81.

Meza-Fajardo, K.C. & Papageogiou, A.S., 2012. Study of the accuracy of the multiaxial perfectly matched layer for the elastic-wave equation, *Bull. Seismol. Soc. Am.*, 102, 2458-2467.

Nataf, F., 2006. A new construction of perfectly matched layers for the linearized Euler equations, *J. Comput. Phys.*, 214, 757–772.

Ping, P., Zhang, Y. & Xu, Y., 2014a. A multiaxial perfectly matched layer (M-PML) for the long-time simulation of elastic wave propagation in the second-order equations, *J. Appl.*

Geophys., 101, 124–135.

Ping, P., Xu, Y., Zhang, Y. & Yang, B., 2014b. Seismic wave modeling in viscoelastic VTI media by using spectral element method, *Earthquake Science*, 27, 553-565.

Roden, J. A. & Gedney, S.D., 2000. Convolution PML (CPML): an efficient FDTD implementation of the CFS-PML for arbitrary media, *Microw. Opt. Technol. Lett.*, 27, 334–339.

Shi, R., Wang, S. & Zhao, J., 2012. An unsplit complex-frequency-shifted PML based on matched Z-transform for FDTD modelling of seismic wave equations, *J. Geophys. Eng.*, 9, 218.

Wang, L. & Liang, C., 2006. A new implementation of CFS-PML for ADIFDTD method, *Microwave Opt. Technol. Lett.*, 48, 1924–1928.

Winton, S.C. & Rappaport, C.M., 2000. Specifying PML conductivities by considering numerical reflection dependencies, *Antennas and Propagation, IEEE*, 48, 1055-1063.

Xie, Z., Komatitsch, D., Martin, R. & Matzen, R., 2014. Improved forward wave propagation and adjoint-based sensitivity kernel calculations using a numerically stable finite-element PML, *Geophysical Journal International*, 198, 1714-1747.

Zeng, C., Xia, J., Miller, R. & Tsoflias, G., 2011. Application of the multiaxial perfectly matched layer (M-PML) to near-surface seismic modeling with Rayleigh waves., *Geophysics*, 76, T43–T52.

Zeng, Y.Q., He, J.Q. & Liu, Q.H., 2001. The application of the perfectly matched layer in numerical modeling of wave propagation in poroelastic media, *Geophysics*, 66, 1258–1266.

Zhang, W. & Shen, Y., 2010. Unsplit complex frequency-shifted PML implementation using auxiliary differential equations for seismic wave modeling, *Geophysics*, 75, T141–T154.

Zhang, Z., Zhang, W. & Chen, X., 2014. Complex frequency-shifted multi-axial perfectly matched layer for elastic wave modelling on curvilinear grids, *Geophys, J. Int*., 198, 140-153.

Zhao, L. & Cangellaris, A.C., 1996. GT-PML: generalized theory of perfectly matched layers and its application to the reflectionless truncation of finite-difference time-domain grids, *IEEE Trans. Microw. Theory. Tech.*, 44, 2555–2563.

Ziolkowski, R.W., 1997. Time-derivative Lorenz material model based absorbing boundary conditions, *IEEE Trans. Antennas Propag.*, 45, 1530–1535.

Tables

Table 1. Parameters of viscoelastic isotropic model*

	Case 1
P wave velocity $V_P(m/s)$	800
S wave Velocity $V_S(m/s)$	200
Mass density $\rho(kg/m^3)$	2000
Poisson's ratio ν	0.47
Relaxation time $\tau_{\varepsilon 1}$ for S	0.0325305
Relaxation time $\tau_{\sigma 1}$ for S	0.0311465
Relaxation time $\tau_{\varepsilon 2}$ for S	0.0032530
Relaxation time $\tau_{\sigma 2}$ for S	0.0031146
Quality factor Q_S	≈ 20
Relaxation time $\tau_{\varepsilon 1}$ for P	0.0332577
Relaxation time $\tau_{\sigma 1}$ for P	0.0304655
Relaxation time $\tau_{\varepsilon 2}$ for P	0.0033257
Relaxation time $\tau_{\sigma 2}$ for P	0.0030465
Quality factor Q_P	≈ 30

*Carcione et al.,1988; Komatitsh and Martin, 2009; Ping et al., 2014a

Table 2. Parameters of anisotropic models*

	Case 2	Case 3
Mass density $\rho(kg/m^3)$	1	7100
$C_{11}(N/m^2)$	4.0	1.65×10^{11}
$C_{12}(N/m^2)$	7.5	5.00×10^{10}
$C_{22}(N/m^2)$	20	6.20×10^{10}
$C_{33}(N/m^2)$	2	3.96×10^{10}
Relaxation time $\tau_{\varepsilon 1}$ for S	0.0325305	0.0325305
Relaxation time $\tau_{\sigma 1}$ for S	0.0311465	0.0311465
Relaxation time $\tau_{\varepsilon 2}$ for S	0.0032530	0.0032530
Relaxation time $\tau_{\sigma 2}$ for S	0.0031146	0.0031146
Quality factor Q_S	≈ 20	≈ 20
Relaxation time $\tau_{\varepsilon 1}$ for P	0.0332577	0.0332577
Relaxation time $\tau_{\sigma 1}$ for P	0.0304655	0.0304655
Relaxation time $\tau_{\varepsilon 2}$ for P	0.0033257	0.0033257
Relaxation time $\tau_{\sigma 2}$ for P	0.0030465	0.0030465
Quality factor Q_P	≈ 30	≈ 30

*Carcione et al.,1988; Matin and Komatitsh, 2009; Meza-Fajardo and Papageorgiou, 2008

Figure Captions

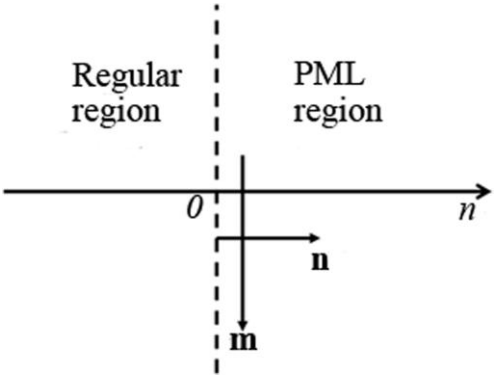

Figure 1. Relation of the regular region and the PML region. The damping vectors **n** and **m** denote normal and parallel to the interfaces, respectively.

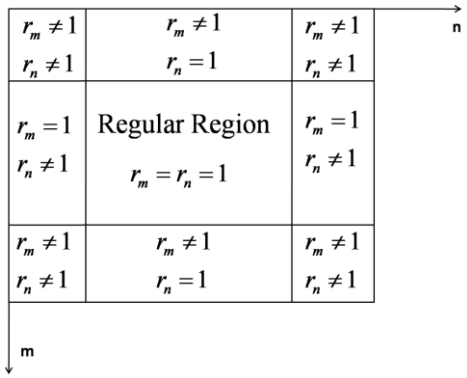

Figure 2. The choice of damping function for the second-order C-PML model.

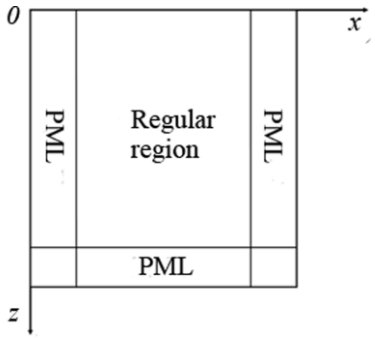

Figure 3. The geometry of a PML model. PMLs are set in both vertical and bottom edges.

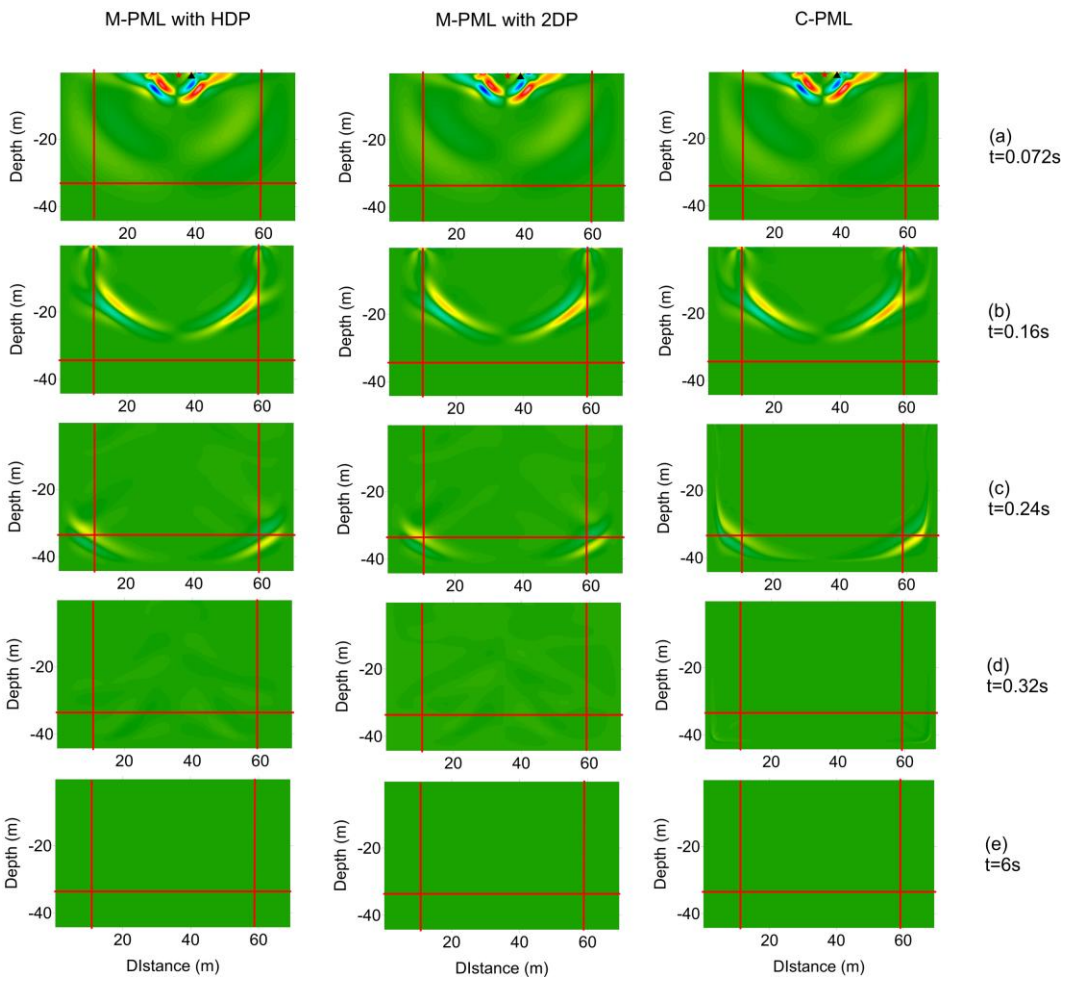

Figure 4. Snapshots of horizontal displacement simulated by SEM in an isotropic viscoelastic medium (Table 1) with high value of Poisson's ratio at (a) t=0.072 s, (b) t=0.16 s, (c) t=0.24 s, (d) t=0.32 s, (e) t=6 s. The red pentacles and black triangles in (a) denote the source and receiver location, respectively. The panels in left and middle columns correspond to the M-PML with high-order and 2nd-order damping profile ($p^{(x/z)}$=$p^{(z/x)}$=0.6), respectively. The right column is for the C-PML. No instability is observed in the M-PMLs and C-PML terminations. Some slight reflections appear from the interfaces between the regular region and M-PML regions.

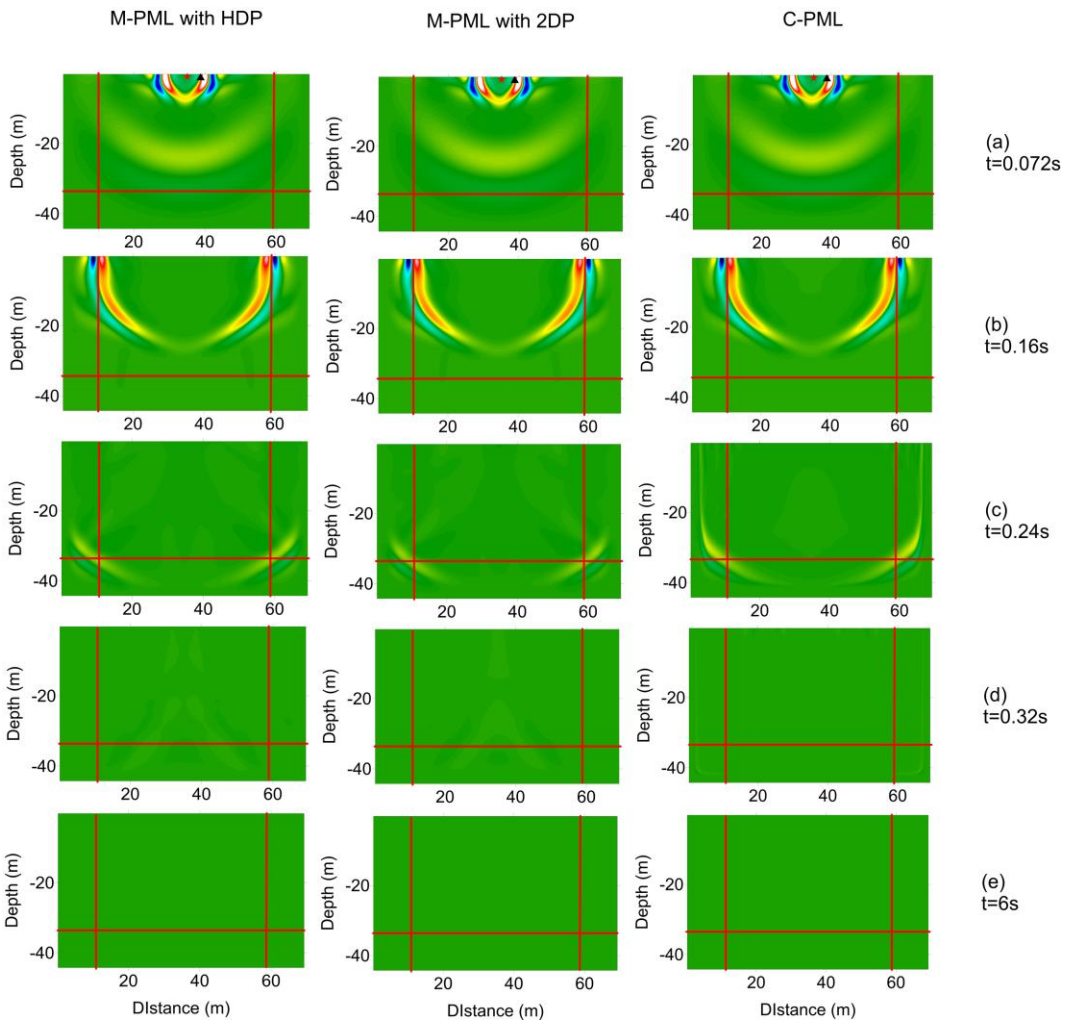

Figure 5. Snapshots of vertical displacement simulated by SEM in an isotropic viscoelastic medium (Table 1) with high value of Poisson's ratio at (a) t=0.072 s, (b) t=0.16 s, (c) t=0.24 s, (d) t=0.32 s, (e) t=6 s. The red pentacles and black triangles in (a) denote the source and receiver location, respectively. The panels in left, middle and right columns correspond to the M-PML with high-order and 2nd-order damping profile ($p^{(x/z)}$=$p^{(z/x)}$=0.6), and the second-order C-PML, respectively. The imperfectly matched properties of the M-PMLs make the reflections from interfaces visible but weak. It is obvious that no unexpected energy occurred from all the boundaries.

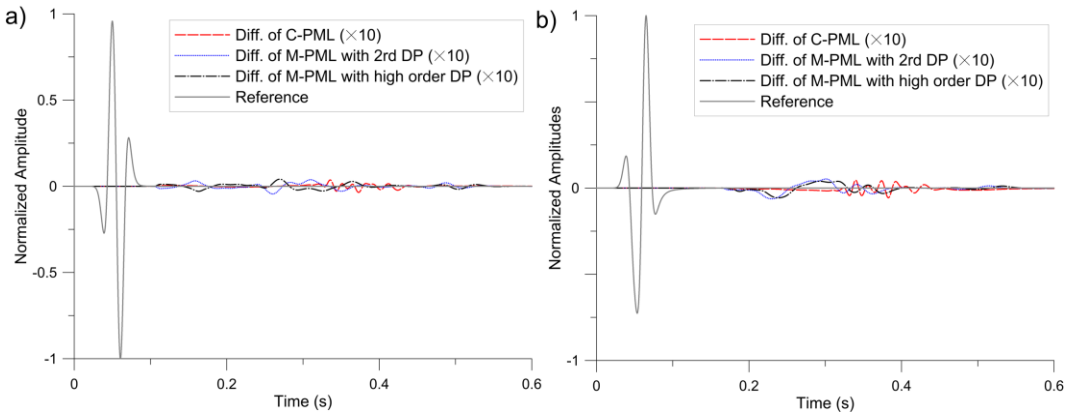

Figure 6. Normalized differences of horizontal (a) and vertical (b) displacements record at (38.75 m, 0.0 m). The reference solutions are computed with the same numerical scheme on a very large mesh with no absorbing boundaries. The differences multiplied by a factor of 10, between the M-PML with 2nd-order (tiny dotted line) or high-order damping profile (dash-dotted line) and the references (solid line). Differences of the M-PMLs exceed that of the C-PML (dotted line) before 0.32 s. The errors in the C-PML increase at late simulation time around 0.32 to 0.45 s.

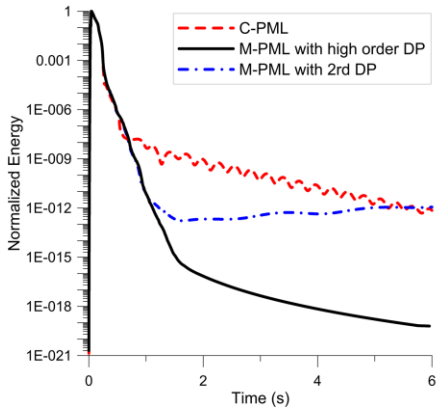

Figure 7. Energy decay with time for the M-PML with high-order and 2nd-order damping profile, and the C-PML in the regular region for the isotropic viscoelastic medium with high value of Poisson's ratio (Table 1).

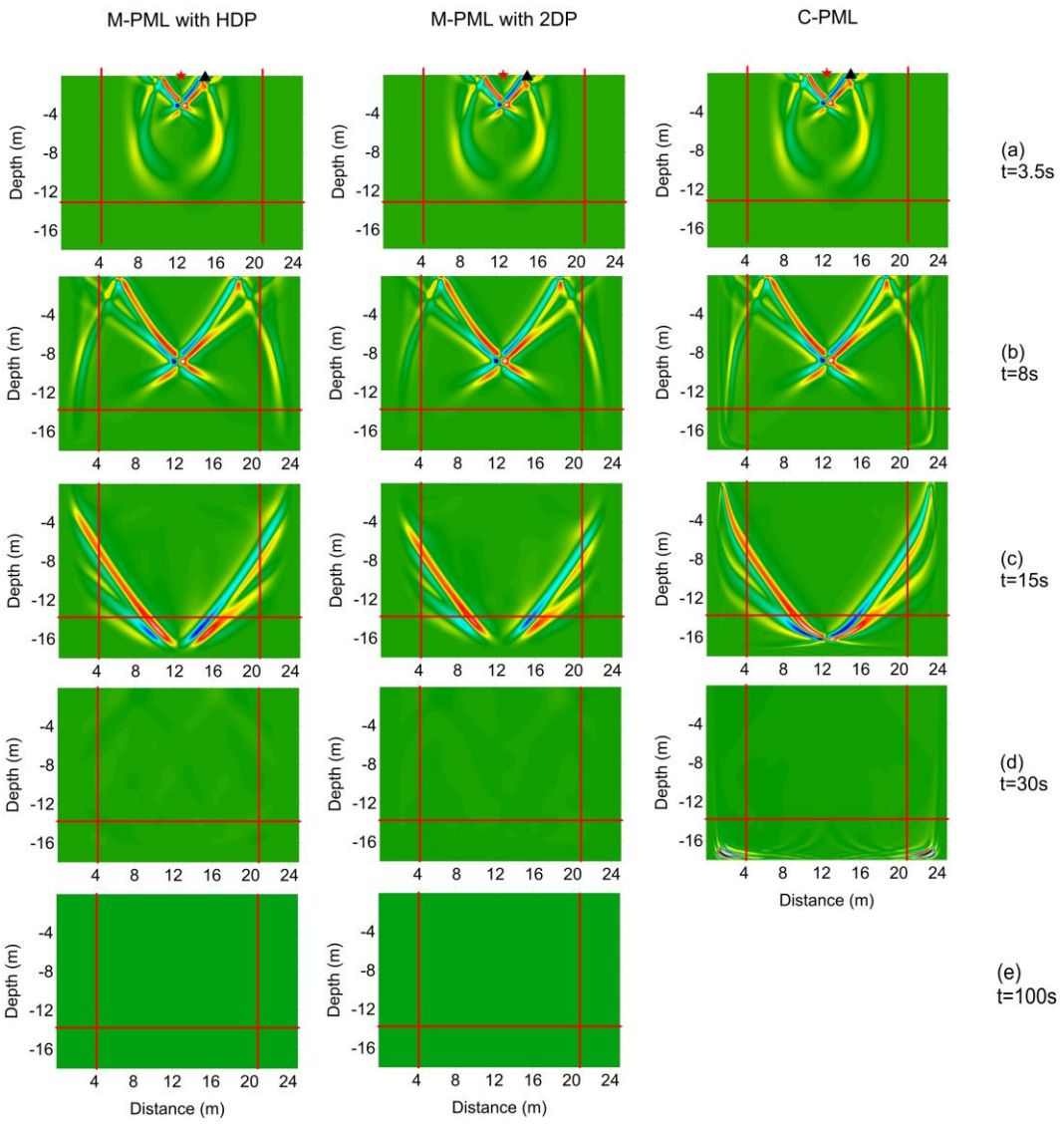

Figure 8. Snapshots of horizontal displacement simulated by SEM in an orthotropic anisotropic viscoelastic medium (Case 2 in Table 2) at (a) t=3.5 s, (b) t=8 s, (c) t=15 s, (d) t=30 s, (e) t=100 s. The red pentacles and black triangles in (a) denote the source and receiver location, respectively. The panels in the left and right columns correspond to the M-PML with high-order and 2nd-order damping profile ($p^{(x/z)}$=0.25, $p^{(z/x)}$=0.3). The right column is for the C-PML, for which the instability appears when the split slow waves propagate into the absorbing regions and outside the model. No instability is observed for the M-PMLs terminations.

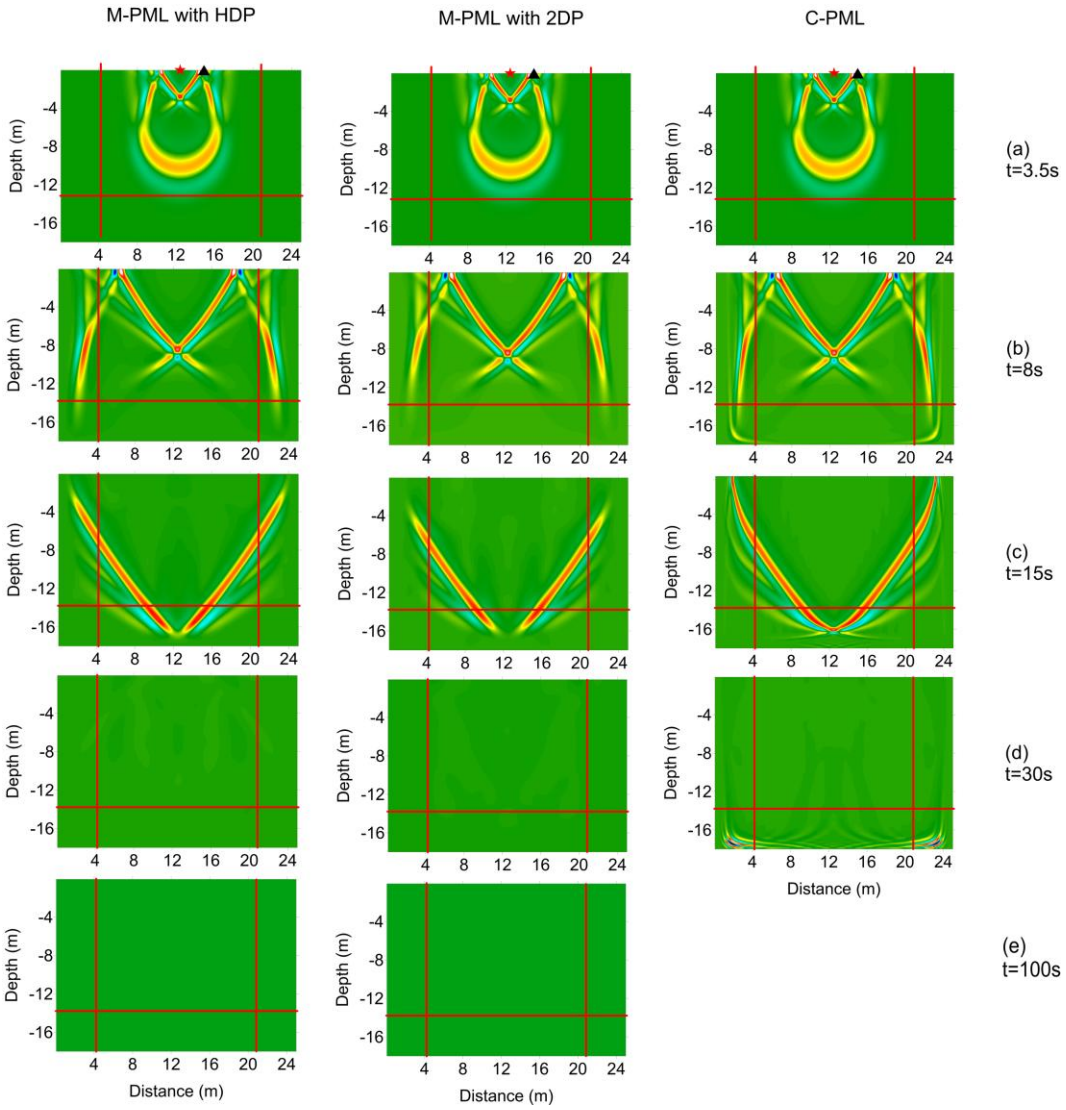

Figure 9. Snapshots of vertical displacement simulated by SEM in an orthotropic anisotropic viscoelastic medium (Case 2 in Table 2) at (a) t=3.5 s, (b) t=8 s, (c) t=15 s, (d) t=30 s, (e) t=100 s. The red pentacles and black triangles in (a) denote the source and receiver location, respectively. The panels in left and right columns correspond to the M-PML with high-order and 2nd-order damping profile ($p^{(x/z)}$=0.25, $p^{(z/x)}$=0.3). The right column is for the C-PML. No instability is observed for the M-PMLs terminations.

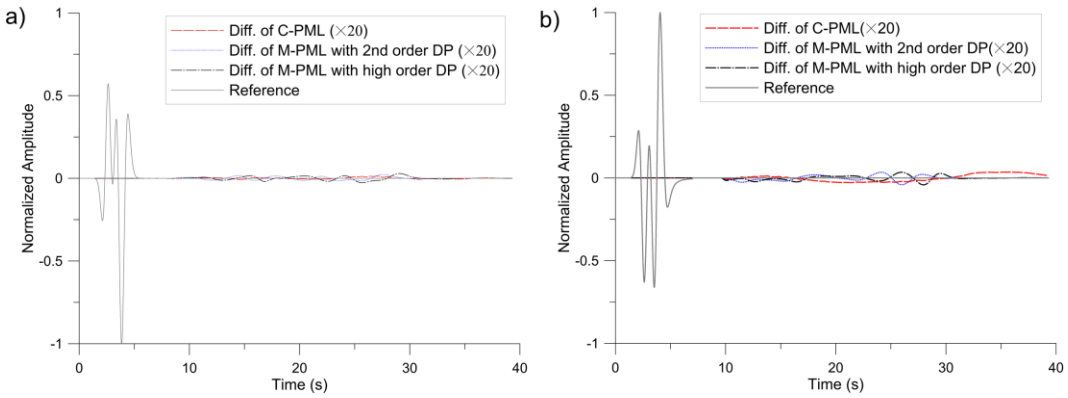

Figure 10. Horizontal (a) and vertical (b) components of normalized differences. The displacements are recorded at (14.91 m, 0.0 m). The differences between the M-PML with 2nd-order (tiny dotted line) or high-order damping profile (dash-dotted line) and the reference (solid line) which are computed with the same numerical scheme on a very large mesh with no absorbing boundaries, are all multiplied by a factor of 20. The errors in the C-PML (dotted line) do not exceed that of the M-PMLs around 10 to 33 s, but are amplified especially in vertical component (b). Meanwhile, these reflections are acceptable and insignificant.

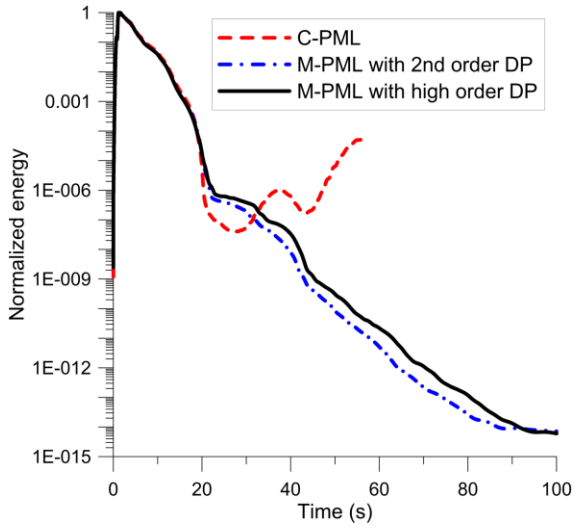

Figure 11. Energy decay with time for the M-PML with high-order and 2nd-order damping profile, and the C-PML in the regular region for the orthotropic anisotropic viscoelastic medium (Case 2 in Table 2).

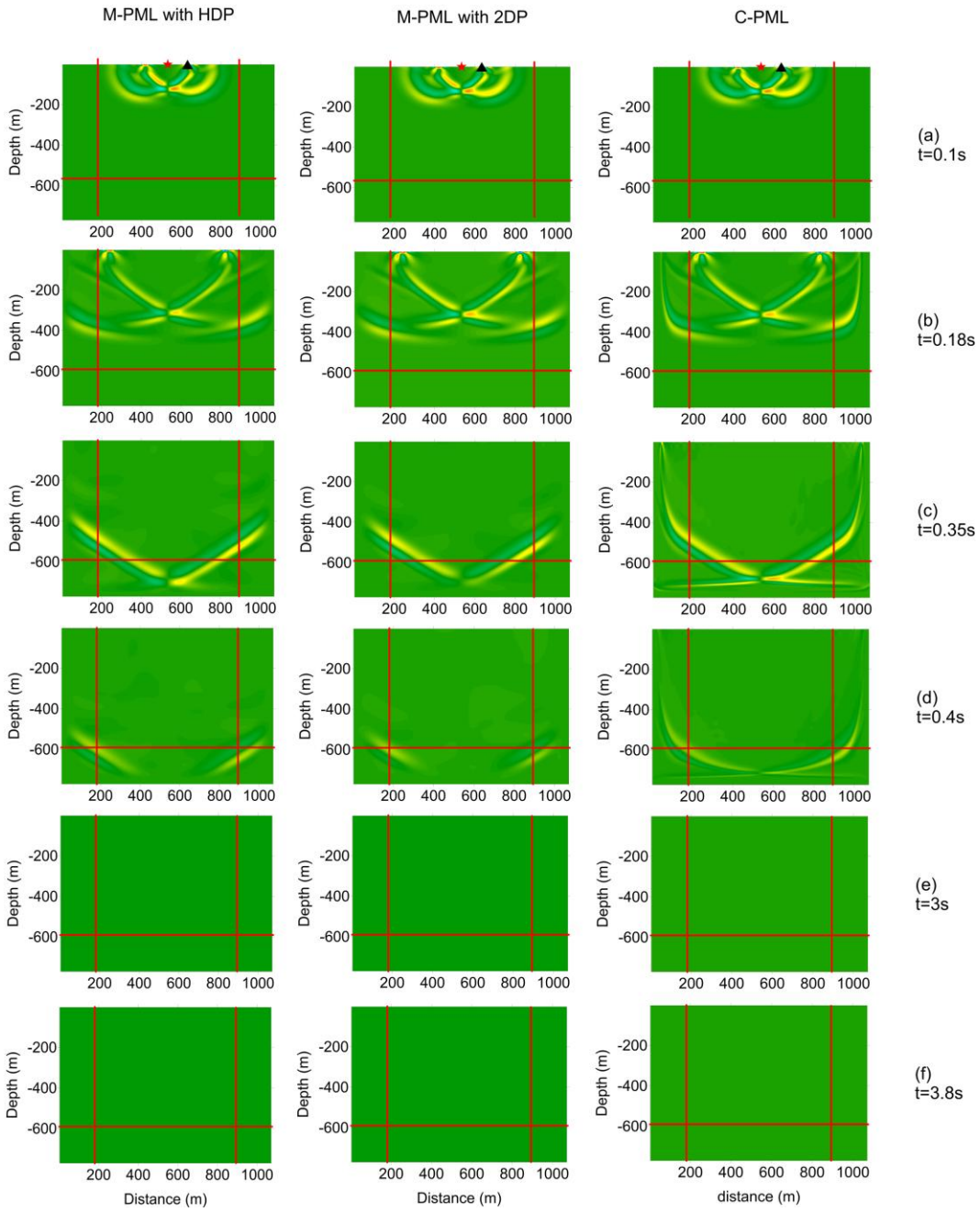

Figure 12. Snapshots of horizontal displacement simulated by SEM in an orthotropic anisotropic viscoelastic medium (Case 3 in Table 2) at (a) t=0.1 s, (b) t=0.18 s, (c) t=0.35 s, (d) t=0.4 s, (e) t=3 s, (f) t=3.8 s. The red pentacles and black triangles in (a) denote the source and receiver location, respectively. Panels in the left, middle and right columns correspond to the M-PML with high-order and 2nd-order damping profile ($p^{(x/z)}$=$p^{(z/x)}$=0.15), and the C-PML, respectively. No instability is observed for all the PMLs.

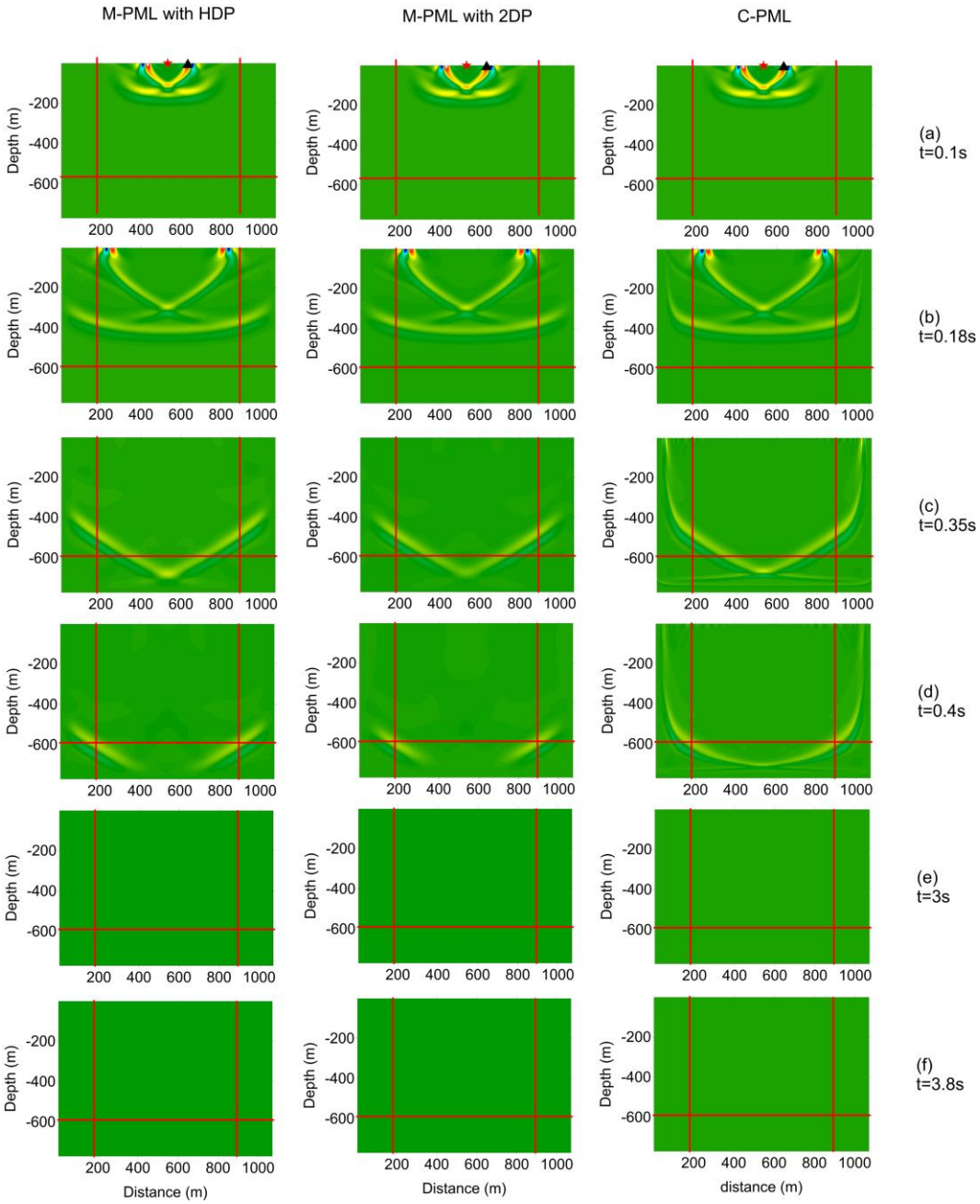

Figure 13. Snapshots of vertical displacement simulated by SEM in an orthotropic anisotropic viscoelastic medium (Case 3 in Table 2) at (a) t=0.1 s, (b) t=0.18 s, (c) t=0.35 s, (d) t=0.4 s, (e) t=3 s, (f) t=3.8 s. The red pentacles and black triangles in (a) denote the source and receiver location, respectively. The panels in left and right columns correspond to the M-PML with high-order and 2nd-order damping profile ($p^{(x/z)}$=0.25, $p^{(z/x)}$=0.3). The right column is for the C-PML. There is no unexpected energy observed for all the PMLs.

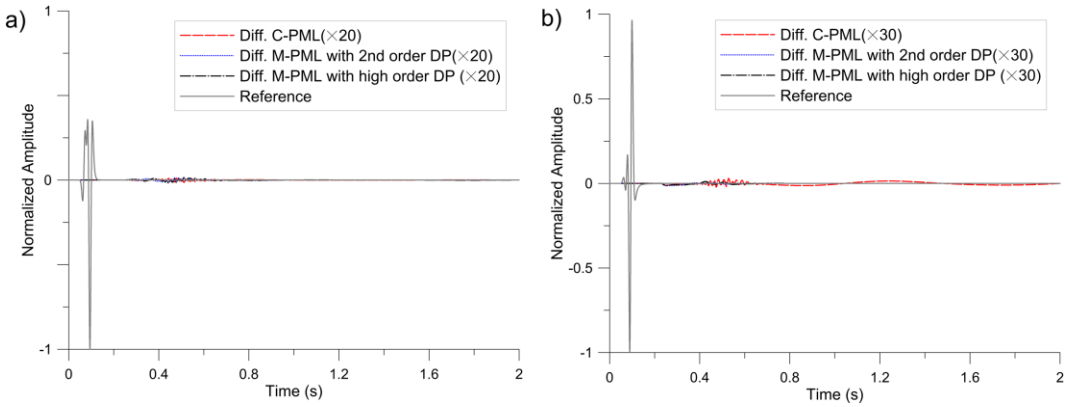

Figure 14. Normalized differences of horizontal (a) and vertical (b) displacement record at (633.0 m, 0.0 m). The horizontal and vertical differences between the M-PML with 2nd-order (tiny dotted line) or high-order damping profile (dash-dotted line) or the C-PML (dotted line) and the reference (solid line) are multiplied by factor of 20 (a) and 30 (b), respectively. The reference solutions are computed with the same numerical scheme on a very large mesh with no absorbing boundaries. The errors in all the PMLs appear at 0.3 s, and become significant after 0.4 s for the C-PML, especially for the vertical component.

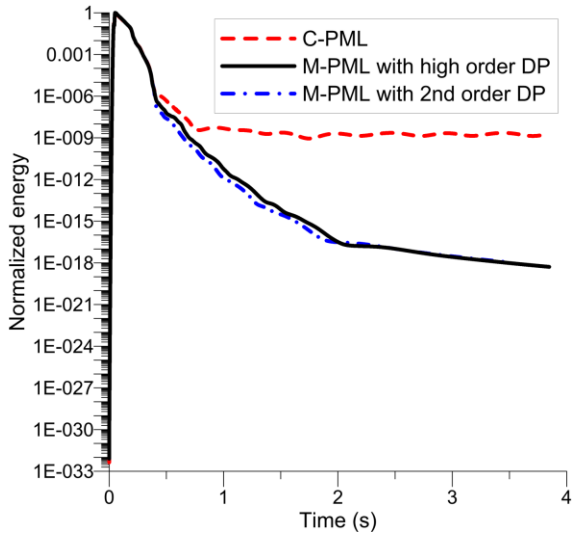

Figure 15. Energy decay with time for the M-PML with high-order and 2nd-order damping profile, and the C-PML in the regular region for the orthotropic anisotropic viscoelastic medium (Case 3 in Table 2).